



HAL
open science

A review of physics-based low-temperature proton-exchange membrane fuel cell models for system-level water and thermal management studies

Pedro Henrique Affonso Nóbrega

► To cite this version:

Pedro Henrique Affonso Nóbrega. A review of physics-based low-temperature proton-exchange membrane fuel cell models for system-level water and thermal management studies. *Journal of Power Sources*, 2023, 558, pp.232585. 10.1016/j.jpowsour.2022.232585 . hal-03966374

HAL Id: hal-03966374

<https://hal.science/hal-03966374>

Submitted on 31 Jan 2023

HAL is a multi-disciplinary open access archive for the deposit and dissemination of scientific research documents, whether they are published or not. The documents may come from teaching and research institutions in France or abroad, or from public or private research centers.

L'archive ouverte pluridisciplinaire **HAL**, est destinée au dépôt et à la diffusion de documents scientifiques de niveau recherche, publiés ou non, émanant des établissements d'enseignement et de recherche français ou étrangers, des laboratoires publics ou privés.

Highlights

A review of physics-based low-temperature proton-exchange membrane fuel cell models for system-level water and thermal management studies

Pedro Henrique Affonso Nóbrega

- Review of low computational cost physics-based PEMFC numerical models.
- Focus on transport phenomena impacting water and thermal management performance.
- Analysis 54 models with different levels of detail and modelling hypotheses.
- Comparison of model validation practices and computational time.

A review of physics-based low-temperature proton-exchange membrane fuel cell models for system-level water and thermal management studies

Pedro Henrique Affonso Nóbrega^a

^a*Mines Paris, PSL University, Centre for processes, renewable energy and energy systems (PERSEE), 06904 Sophia Antipolis, France*

Abstract

Water management and thermal management are essential for the design and operation of low-temperature proton-exchange membrane fuel cells and demand a deep understanding of the fuel cell system behavior. System-level studies require fast and simple numerical models, a challenge given the complexity of the transport phenomena involved. Numerous models exist in the literature, with different levels of complexity and different hypotheses aiming at simplifying the representation of transport phenomena. This review presents different hypotheses and modelling approaches adopted in low computational cost physics-based proton-exchange membrane fuel cell models, with a focus on aspects related to water and thermal management. We also present modelling approaches for auxiliary system components, validation practices and compare the computational efficiency of different models. We conclude that rather than developing new models from scratch, a strong effort on the validation of the existing models is needed, with the development of a standard validation procedure.

Keywords: Proton-exchange membrane, Fuel cell, Physics-based model, Water management, Thermal management

Email address: pedro.affonso_nobrega@minesparis.psl.eu
(Pedro Henrique Affonso Nóbrega)

Nomenclature

Abbreviations

AC	Along-the-channel
BP	Bipolar plate
CL	Catalyst layer
CSTR	Continuously-stirred tank reactor
DM	Diffusion medium
EIS	Electrochemical impedance spectroscopy
GC	Gas channel
GDL	Gas diffusion layer
IP	In-plane
MEA	Membrane-electrode assembly
MPL	Micro-porous layer
NTU	Number of transfer units
OCV	Open-circuit voltage
PEM	Proton-exchange membrane
PFSA	Perfluorinated sulfonic acid
RH	Relative humidity
RT	Real time
TP	Through-plane

Greek symbols

α	Transfer coefficient, -
η	overpotential, V
λ	Membrane/ionomer water content, -
μ	Dynamic viscosity, Pa s
ρ	Density, kg m ⁻³
σ_l	Liquid water surface tension, N m ⁻¹
σ_{memb}	Membrane conductivity, $\Omega^{-1} \text{ m}^{-1}$
θ	Contact angle, -
ε	Porosity, -
ε_p	Percolation threshold, -
ξ	Electroosmotic drag coefficient, -

Roman symbols

\dot{m}	Mass flow rate, kg s ⁻¹
\dot{Q}	Gas flow rate, m ³ s ⁻¹
\dot{Q}	Heat source, W
A	Surface area, m ²
a	Water activity, -
C	Heat capacity, J kg ⁻¹
c	Concentration, mol m ⁻³
c_f	Sulfonic acid concentration, mol m ⁻³
D	Diffusion coefficient, m ² s ⁻¹
D_λ	Membrane water diffusion coefficient, m ² s ⁻¹
D_T	Thermoosmotic diffusion coefficient, mol m ⁻¹ K ⁻¹ s ⁻¹
E	Potential, V
F	Faraday's constant, 96 485 C mol ⁻¹
h	Heat transfer coefficient, W K ⁻¹ m ⁻²
h	Specific enthalpy, J kg ⁻¹
i	Current density, A m ⁻²

i_0	Exchange current density, A m ⁻²
K	Permeability, m ²
k_{abs}	Absorption/desorption rate coefficient, m s ⁻¹ or mol m ⁻² s ⁻¹
M	Molar mass, kg mol ⁻¹
N_{cells}	Number of cells in the stack, -
P	Power, W
p	Pressure, Pa
p_c	Capillary pressure, Pa
q	Mass flux, kg m ⁻²
R	Universal gas constant, 8.3145 J mol ⁻¹ K ⁻¹
r	Resistivity, $\Omega \text{ m}$
r_{H^+}	Protonic resistivity, $\Omega \text{ m}$
r_{el}	Electrotonic resistivity, $\Omega \text{ m}$
S	Entropy, J mol ⁻¹ K ⁻¹
s	Liquid water saturation, -
S_k	Mass source of species k , kg s ⁻¹
S_T	Volume heat source, J s ⁻¹ m ⁻³
s_{ice}	Ice saturation, -
T	Temperature, K
t	Time, s
t_i	Thickness of layer i , m
V	Voltage, V
v	Velocity, m s ⁻¹

Subscripts and superscripts

0	Standard state
memb	Membrane
act	Activation
amb	Ambiant
an	Anode
ca	Cathode
conc	Concentration
cool	Cooling
eff	Effective
el	Electric
eq	Equilibrium
g	Gas
in	Inlet
i	Layer i
k	k -th segment along the channel
k	Species k
l	Liquid
ohm	Ohmic
opt	Optimum
out	Outlet
rev	Reversible
st	Stack
th	Thermal
w	Water

1. Introduction

Fuel cells are devices that allow the conversion of hydrogen and oxygen into electricity, heat and water by electrochemical reactions. Being so, they are essential elements for the use of hydrogen as an energy vector. In particular, low-temperature proton-exchange membrane fuel cells are viewed today as a promising technology for applications in transportation (buses, trucks, trains, auxiliary power units for airplanes) and small-scale distributed power generation, both stationary and portable [1]. However, high cost and low durability of the equipment, as well as integration issues in some vehicle applications still hinder a wider adoption of fuel cells. In order to reduce these barriers, improvements in the design and operation of fuel cell systems are needed.

Water and thermal management of fuel cells are topics where there is room for such improvements. The goal of water management is to keep the proton-exchange membrane hydrated while avoiding excessive water inside the cells [2]. Indeed, the perfluorinated sulfonic acid membranes used in low-temperature PEM fuel cells need to be hydrated to effectively conduct protons and fulfill their role as an electrolyte. If they dry, their proton conductivity decreases, leading to an increased heat release and a decrease of the fuel cell efficiency. Heat release may lead to a local temperature increase, which will, in turn, intensify the membrane drying in a process leading to the irreversible degradation of the membrane. On the other hand, excessive water inside the cell may lead to condensation and the obstruction of gas transport by liquid water accumulated in the porous layers, a phenomenon known as flooding [3]. Concerning thermal management, its goal is to evacuate the heat generated by the fuel cell while keeping an appropriate and homogeneous temperature of operation. Thermal management of low-temperature fuel cells is particularly challenging as their operating temperature is around 80 °C. It is more difficult to dissipate heat at this temperature than in the case of an internal combustion engine operating around 400 °C [4]. Water and thermal management are intimately connected: an increase of the operating temperature will favor water evaporation and membrane drying, while a decrease will favor condensation and flooding. In turn, water evaporation or condensation will absorb or release a significant amount of heat. Water and thermal management are also related to the startup and operation of fuel cells at freezing temperatures, where the solidification of liquid water inside the cell may bring several issues [5].

Water and thermal management of fuel cells require or are impacted by a number of peripherals that contribute significantly to the fuel cell system cost [6]. Those are part of the air supply, fuel supply and cooling sub-systems. We can cite as examples:

- air supply/cathode sub-system: compressor or blower, membrane humidifier, back-pressure valve;
- fuel supply/anode sub-system: hydrogen recirculation pump (or ejector), water separator, purge valve;
- cooling sub-system: cooling pump, three-way valve, radiators.

Membrane humidifier and radiators, in particular, can be voluminous and bring integration difficulties. Valves, air compressor/blower and pumps must be controlled in a way that optimizes performance and durability of the fuel cell under the different expected operating conditions [7]. System-level studies, where all those peripherals, their behavior and their interactions are taken into account are therefore fundamental for improving the design and operation of fuel cell systems from a water and thermal management standpoint.

But such system-level studies require numerical models able to simulate the behavior of the fuel cell system with a sufficiently low computational cost. Indeed, one should be able to simulate with a reasonable computational time the operation of the fuel cell system over time intervals corresponding to load cycles encountered in potential applications, such as vehicle driving cycles. These may last from several minutes to several hours. Moreover parametric studies and optimization algorithms require running simulation cases several times, with the computational cost increasing even more.

Detailed models for PEM fuel cells are, however, too computationally expensive for those kind of studies. Indeed, these detailed models are based on the solution of conservation equations for mass, momentum, species (H_2 , O_2 , N_2 and H_2O in its different phases), heat and charge (both positive and negative) [1, 8]. These equations take the form of partial differential equations, in some cases containing highly non-linear terms, which must be discretized and solved in both time and space. Even solving such a detailed model on only two dimensions such as in the case of Goshtasbi *et al.* [9] can take, depending on the conditions, between 5 and 12 hours to simulate 340 s of the PEM fuel cell behavior on a desktop computer (that means between 50 and 130 times slower than real time). The 2D+1D model of Nandjou *et al.* [10] take 6 hours to calculate a single steady-state operating point.

But the computational cost is not the only drawback of such detailed models. Complexity of the model also brings difficulties into its use in fuel cell system development. The more complex the model is, the more time is needed to implement and maintain it, to setup simulation cases, to debug errors and to post-treat and interpret results. Further, complex models often require a long list of model parameters, some of which have been obtained for conditions or materials different from those under study, some of which are highly uncertain and some of which are not available at all, thus requiring potentially long and costly experimental work. Besides, uncertainty in model parameters can easily curtail the accuracy gained by using a more complex model. The works by Jiang *et al.* [11] and Vetter and Schumacher [12, 13] are particularly enlightening on how uncertainty on key parameters for PEM fuel cell models can have a strong impact on the results. For all those reasons, complex models are not suited to develop fuel cell systems in an agile way.

Obtaining faster and simpler models for PEM fuel cells can therefore accelerate the PEM fuel cell system development. But it requires simplifying hypotheses, since the phenomena involved in the fuel cell operation are complex and encompass multiple scales in space and time. The literature on PEM fuel

cell modelling contain plenty of proposals of simplified models that can be used for system-level studies. Those models adopt a wide variety of hypotheses and approaches that aim to limit the number of equations, the number of points on which the solution is sought (both in space and time dimensions), the evaluation of computationally-intensive non-linear functions or the coupling between different phenomena involved. Many of these hypotheses concern the transport of reactant gases, water in its different phases and heat inside the fuel cells. As a consequence, the impact of these hypotheses is of great importance for those interested in water and thermal management of fuel cells. In spite of that, to the author's knowledge, little has been done to identify the impact of each individual hypothesis on the accuracy of the model and the reduction of the computational cost, as well as the domain of validity of each hypothesis. Due to the complexity of the phenomena involved and the variety of hypotheses and models encountered in the literature, undertaking that analysis in a systematic way is not an easy task. In this review, we propose a first step towards that goal: a presentation of the different hypotheses adopted in system-level and/or control-oriented PEM fuel cell models available in the literature.

In the last ten years, several review papers concerning fuel cell modelling have been published. The review of Weber *et al.* [14] focus on the modelling of transport phenomena in PEM fuel cells, with a very good presentation of the basic governing equations for mass, charge and energy transport and of phenomena occurring in the catalyst layer, for which the reader is referred. The review of Andersson *et al.* [8] focuses on the modelling of multi-phase flow in the gas diffusion layers and gas channels, presenting different computational approaches at the cell scale and a valuable discussion on the different transport properties in the GDL. The reviews of Jiao's group on water transport [2], cold start [5], gas diffusion layers [15] and thermal management [4] also contain some modelling aspect and are an important starting point for those interested in water and thermal management of PEM fuel cells. The review of Jahnke *et al.* [7] is more general and covers the different modelling scales from atomistic to system level, with a focus on the modelling of degradation phenomena. More recently, Zhao *et al.* [16] review fuel cell modelling real-time control, looking into both low-dimension (from 0D to 1D+1D) physics-based models and data-driven models. As Zhao *et al.*, we focus on low-dimension models which can simulate the fuel cell performance with lower computational cost, allowing for system-level and/or control-oriented studies. But more specifically, we concentrate our review on modelling aspects and hypotheses related to the study of fuel cell water and thermal management.

2. Modelling the PEM fuel cell

Fuel cell models can be classified according to the spatial dimensions considered. The so-called 0D models consider the anode and the cathode as a single control volume each behaving like a continuously-stirred tank reactor, without any spatial consideration. A typical 0D model is schematized in figure 1

extracted from Ritzberger *et al.* [64]. 1D models adopt a spatial discretization with more than one control volume along either the flow channel (in-plane) direction or the through-plane direction of the cell. 1D+1D models have more than one control volume for each of the flow channel and through-plane directions, but without any flux in the in-plane direction of the porous layers, taking advantage of the planar geometry of the cell and the much smaller dimension in the through-plane direction. By doing so, 1D+1D models decouple the solution of adjacent through-plane transport equations, leading to faster simulations than with equivalent 2D models where transport in the in-plane direction is solved. The scheme of the 1D+1D model proposed by Yang *et al.* [58] is presented in figure 2. 2D+1D models work in the same way but consider two-dimensional gas flow channel arrangements, while 2D and 3D models take into account in-plane fluxes. Fuel cell models are also classified as transient or steady-state depending on the consideration of dynamic effects. The so-called quasi-steady approach use steady-state equations which are solved for each time step.

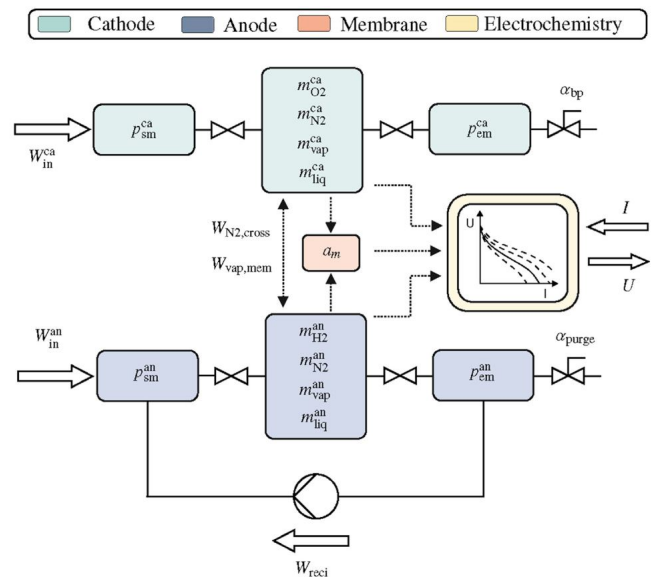


Fig. 1. Schematics of the 0D model used by Ritzberger *et al.* [64]. (Reproduced from Ritzberger *et al.* [64]).

In 2004, Pukrushpan *et al.* [17] proposed perhaps the first control-oriented 0D fuel cell system model taking into account the transient effects of oxygen and hydrogen partial pressures, stack temperature and membrane water content on the stack voltage. The authors clearly state that their model "is useful in showing the behavior of fuel cell systems qualitatively, rather than quantitatively". Several works presented control-oriented models in the following years [20, 22, 28, 30, 35, 36] while paying increasing attention to the control of the stack temperature and the membrane water content. In particular, del Real *et al.* [20] developed a two-phase 0D model which was able to reproduce the transient behaviour of a Ballard Nexa 1.2 kW PEM fuel cell system. In the same period, several steady-state models were also developed with along-the-channel [21], through-plane [23, 34] or even 2D dis-

Table 1

Classification of the main models reviewed in this work.

Pukrushpan <i>et al.</i> , 2004 [17]	Transient	0D	Single-phase	Isothermal
Khan and Iqbal, 2005 [18]	Steady-state	0D	Single-phase	Isothermal
Bao <i>et al.</i> , 2006 [19]	Transient	1D	Two-phase	Isothermal
Del Real, 2007 [20]	Transient	0D	Two-phase	Isothermal
Huisseune <i>et al.</i> , 2008 [21]	Steady-state	1D (AC)	Single-phase	Non-isothermal
Vasu <i>et al.</i> , 2008 [22]	Transient	0D	Single-phase	Isothermal
Falcão <i>et al.</i> , 2009 [23]	Steady-state	1D (TP)	Single-phase	Non-isothermal
Gerteisen <i>et al.</i> , 2009 [24]	Steady-state	1D (TP)	Two-phase	Non-isothermal
Jiao and Li, 2009 [25]	Transient	3D	Two-Phase	Non-isothermal
Karnik <i>et al.</i> , 2009 [26]	Transient	0D	Single-phase	Isothermal
Kim <i>et al.</i> , 2010 [27]	Transient	0D	Single-phase	Isothermal
Mangold <i>et al.</i> , 2011 [28]	Transient	0D	Two-phase	Isothermal
Schultze and Horn, 2011 [29]	Transient	0D	Two-phase	Isothermal
Ziogou <i>et al.</i> , 2011 [30]	Transient	0D	Two-phase	Isothermal
Damour <i>et al.</i> , 2012 [31]	Transient	0D	Single-phase	Isothermal
Hosseinzadeh <i>et al.</i> , 2013 [32]	Steady-state	0D	Single-phase	Isothermal
Chaudhary <i>et al.</i> , 2014 [33]	Transient	2D	Two-phase	Non-isothermal
Kim <i>et al.</i> , 2014 [34]	Steady-state	1D (TP)	Two-phase	Isothermal
Liso <i>et al.</i> , 2014 [35]	Transient	0D	Two-phase	Isothermal
Strahl <i>et al.</i> , 2014 [36]	Transient	0D	Two-phase	Isothermal
Zhou <i>et al.</i> , 2014 [37]	Transient	1D (TP)	Two-phase	Non-isothermal
Fly, 2015a [38]	Transient	0D	Two-phase	Isothermal
Kang, 2015 [39]	Transient	2D+1D (TP)	Two-phase	Non-isothermal
Kang and Min, 2016 [40]	Transient	1D (TP)	Two-phase	Non-isothermal
Robin <i>et al.</i> , 2015 [41]	Transient	2D+1D (TP)	Two-phase	Non-isothermal
Zhao <i>et al.</i> , 2015 [42]	Transient	0D	Single-phase	Isothermal
Abdin <i>et al.</i> , 2016 [43]	Transient	0D	Single-phase	Isothermal
Goshtasbi <i>et al.</i> , 2016 [44]	Transient	1D+1D	Two-phase	Non-isothermal
Headley <i>et al.</i> , 2016 [45]	Transient	1D (AC)	Single-phase	Isothermal
Liso <i>et al.</i> , 2016 [46]	Steady-state	1D (TP)	Two-phase	Isothermal
Salva <i>et al.</i> , 2016 [47]	Steady-state	1D (TP)	Two-phase	Non-isothermal
Schultze and Horn, 2016 [48]	Transient	0D	Single-phase	Isothermal
Tang <i>et al.</i> , 2017 [49]	Transient	1D+1D	Two-phase	Non-isothermal
Futter <i>et al.</i> , 2018 [50]	Transient	2D	Two-phase	Non-isothermal
Jiang <i>et al.</i> , 2018 [11]	Steady-state	1D (TP)	Two-phase	Non-isothermal
Qin <i>et al.</i> , 2018 [51]	Steady-state	2D (IP)	Single-phase	Non-isothermal
Sun <i>et al.</i> , 2018 [52]	Transient	0D	Single-phase	Isothermal
Wang <i>et al.</i> , 2018 [53]	Transient	1D+1D	Two-phase	Non-isothermal
De Campo, 2019 [54]	Transient	0D	Two-phase	Isothermal
Han <i>et al.</i> , 2019 [55]	Steady-state	1D (TP)	Single-phase	Isothermal
Lazar <i>et al.</i> , 2019 [56]	Transient	1D (TP)	Single-phase	Isothermal
Vetter and Schumacher, 2019 [57]	Steady-state	1D (TP)	Two-phase	Non-isothermal
Yang <i>et al.</i> , 2019 [58, 59]	Transient	1D+1D	Two-phase	Non-isothermal
Chen <i>et al.</i> , 2020 [60]	Transient	0D (scalable)	Two-phase	Non-isothermal
Goshtasbi <i>et al.</i> , 2020 [61]	Transient	1D+1D	Two-phase	Non-isothermal
Hoeflienger and Hofmann, 2020 [62]	Steady-state	0D	Single-phase	Isothermal
Ritzberger <i>et al.</i> , 2020 [63, 64]	Transient	0D	Two-phase	Isothermal
Wang <i>et al.</i> , 2020 [65]	Transient	0D	Single-phase	Isothermal
Fu <i>et al.</i> , 2021 [66]	Transient	0D	Two-phase	Isothermal
Schröder <i>et al.</i> , 2021 [67]	Steady-state	1D (TP)	Two-phase	Isothermal
Xing <i>et al.</i> , 2021 [68]	Transient	0D	Single-phase	Isothermal
Xu <i>et al.</i> , 2021 [69]	Transient	1D (TP)	Two-phase	Isothermal
Gong <i>et al.</i> , 2022 [70]	Transient	1D+1D	Two-phase	Non-isothermal
Striednig <i>et al.</i> , 2022 [71, 72]	Steady-state	0D	Single-phase	Isothermal

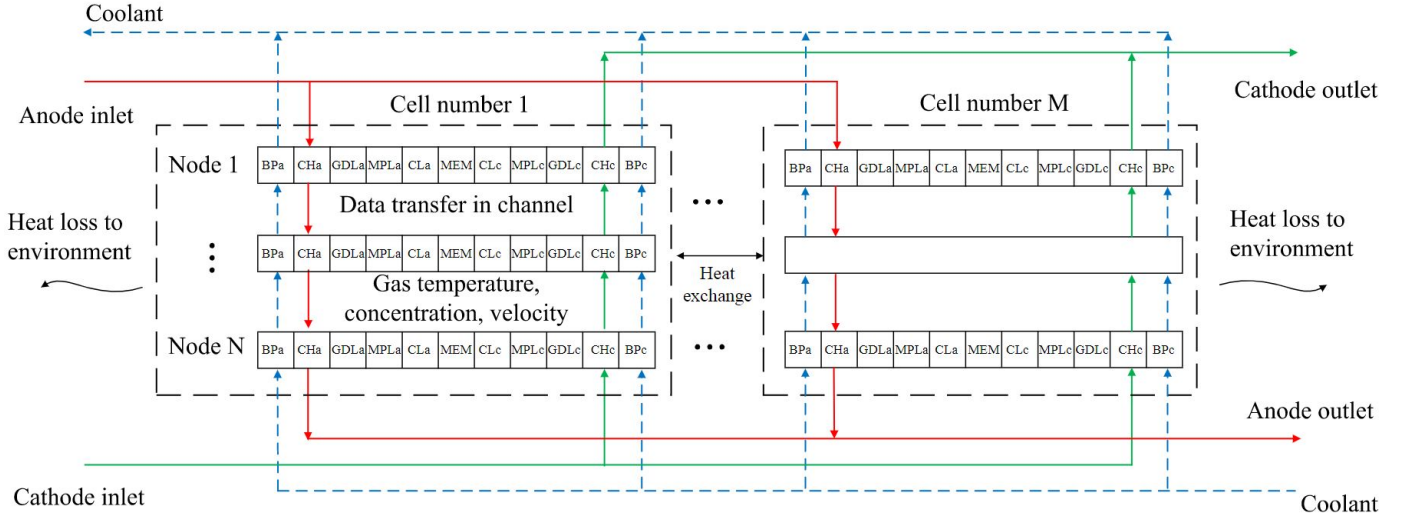


Fig. 2. Schematics of the 1D+1D model from Yang *et al.* [58]. (Reproduced from Yang *et al.* [58] with permission from Elsevier).

cretizations, as they allowed to account for spatial dimensions and heat transfer effects which were neglected in 0D models. With time and the improvement of computational capabilities, some models started to combine both detailed spatial discretization and dynamic operation [37, 41, 49, 50, 58, 61]. Models also started to include two-phase effects more often [11, 33, 36, 37, 39, 40, 47, 58, 61, 67, 69, 70], although those were already present in the model proposed by del Real *et al.* [20]. More recently, some authors came back to simpler models (0D and/or steady-state) in order to reduce the computational time and make faster system-level optimization [62, 67], sensitivity analyses [11, 71] and model calibration [63, 64]. In some cases, analytical solutions of governing equations are included to further reduce computational time [11, 69].

Table 1 lists the PEM fuel cell models mentioned in this work and how they could be classified according to the consideration of dynamic effects (steady-state or transient models), the spatial dimensions (from 0D to 3D), as well as the consideration of two-phase phenomena and of temperature heterogeneity (isothermal or non-isothermal). In the following, we will see how those models represent the cell voltage, the transport phenomena in the different layers of the membrane-electrode assembly and in the gas flow channels and associated spatial effects at the cell and stack scales.

2.1. Cell voltage

Most often, the goal of fuel cell models is to predict the operating voltage for a given current density. Models calculate the cell voltage from the current densities either by solving charge conservation equations or by adopting semi-empirical parametrizations. For those solving charge conservation equations, both proton and electron conservation are considered in the through-plane direction. Proton conservation is solved in the catalyst layers and membrane and electron conservation in the catalyst layers, DM and bipolar plates. Examples of

models considering charge conservation equations are found in [24, 25, 33, 50, 55, 57]. In the majority of the models reviewed in this work, the semi-empirical parametrization of the cell voltage is used, for its simplicity and computational efficiency. Further, its parameters can be more easily fitted to experimental data. The cell voltage can be obtained by subtracting activation, ohmic and concentration overpotentials terms from the reversible potential :

$$V_{cell} = E_{rev} - \eta_{act} - \eta_{ohm} - \eta_{conc} \quad (1)$$

The reversible potential is calculated with the Nernst equation:

$$E_{rev} = E_{rev}^0 + \frac{\Delta S^0}{2F}(T - T_0) + \frac{RT}{2F} \ln \left[\left(\frac{p_{O_2}}{p_0} \right)^{0.5} \left(\frac{p_{H_2}}{p_0} \right) \right] \quad (2)$$

with the standard conditions $p_0 = 1 \text{ atm}$, $T_0 = 298.15 \text{ K}$, $E_{rev}^0 = 1.229 \text{ V}$ and $\Delta S^0 = 165 \text{ J mol}^{-1} \text{ K}^{-1}$.

2.1.1. Activation overpotential

The activation overpotential is generally represented by a Butler-Volmer formulation [25, 33, 49, 50, 57] or the simpler Tafel equation [19, 23, 24, 34, 36–40, 43, 44, 47, 53, 55, 58, 59, 61, 62, 67, 69–71], valid for large values of η_{act} and negligible mass transfer resistance, given by:

$$\eta_{act} = \frac{RT}{2\alpha F} \ln \left(\frac{i}{i_0} \right) \quad (3)$$

The exchange current density i_0 can be a constant or a function of the temperature and the oxygen concentration. An empirical crossover current term can be added to the cell current density in equation 3 to account for the crossover of gas species across the membrane. As an alternative to the Tafel equation, Jiang *et al.* [11] solve the charge conservation equations analytically to obtain a parametrization for the activation overpotentials. The

semi-empirical parametrization of the activation overpotential proposed by Amphlett *et al.* [73] is also extensively used in fuel cell models [18, 21, 27, 29–32, 48, 54, 60, 65, 66, 68]. It describes the activation overpotential as a linear combination of four terms which can be fitted to experimental data:

$$\eta_{act} = \xi_1 + \xi_2 T + \xi_3 T \ln(c_{O_2}^*) + \xi_4 T \ln i \quad (4)$$

where the oxygen concentration at the cathode gas-liquid interface $c_{O_2}^*$ is obtained from the Henry's law and ξ_i are the fitting coefficients. Nevertheless, other alternative parametrizations are also used by different authors [17, 20, 22, 35, 41, 45, 56, 63]. Very often the anode activation overpotential is neglected as the hydrogen oxidation reaction is much faster than the oxygen reduction reaction.

2.1.2. Ohmic overpotential

The ohmic overpotential is due to both protonic and electronic resistances across the different layers of the cell and can be written:

$$\eta_{ohm} = r_{ohm} i = (r_{H^+} + r_{el}) i \quad (5)$$

Protonic resistances occur in the catalyst layers and the membrane, while electronic resistances occur across the catalyst layers, the MPL and GDL and the bipolar plates. The protonic resistance is generally dominant and is a strong function of the membrane water content in the perfluorinated sulfonic acid membranes used in low-temperature PEMFC. Most models [11, 17, 19, 23–25, 29, 32–35, 37–40, 43, 44, 47, 49, 50, 54, 55, 67, 69] still use the empirical relation for the conductivity of a Nafion 117 membrane obtained back in 1991 by Springer *et al.* [74]:

$$\sigma_{memb} = (0.005139\lambda - 0.00326) \times \exp\left[1268\left(\frac{1}{303} - \frac{1}{T}\right)\right] \quad (6)$$

with σ_{memb} in $\Omega^{-1} \text{cm}^{-1}$ and T in Kelvins. Some authors multiply equation 6 by a tuning factor [35, 40] or fit its different parameters to their own experimental data [41, 45, 63]. Mann *et al.* [75] proposed some correction terms to equation 6 that are adopted by several works [18, 27, 42, 54, 60, 65, 66, 68]. Other less commonly used parametrizations are the one proposed by Amphlett *et al.* [73] and used by [21, 30], defined as:

$$\sigma_{memb} = \xi_5 + \xi_6 T + \xi_7 i \quad (7)$$

or a more complex equation proposed by Weber and Neumann [76] and used by [56, 57]. Some specific parametrizations can also be found in [61, 62, 71]. Given the membrane conductivity, its protonic resistance can be calculated based on the membrane thickness. Calculating the protonic conductivity of the catalyst layer require the knowledge of catalyst properties such as the ionomer volume fraction, catalyst layer thickness and tortuosity. This is done by a few works [24, 25, 33, 37, 49, 50, 61, 67, 69] but most neglect the catalyst layer protonic conductivity. The cell electronic conductivity can be calculated from the series association of the electronic resistances of the different porous layers and bipolar plate

[33, 37, 43, 44, 47, 50, 58, 59, 65, 70] and sometimes a contact resistance [27, 41, 44, 47, 60, 61, 63] which is often a fitted parameter lumping all the electronic resistances of the cell. However, the majority of studies consider only the protonic resistance of the membrane in the ohmic overpotential. That might be a good approximation for thick membranes. But with the current trend for the use of thinner membranes, specially for mobility applications, the protonic resistances of the catalyst layers and the electronic resistances become more and more significant for the fuel cell performance. Finally, some authors [20, 22, 31, 36, 42, 48] consider the ohmic resistance as a constant parameter that can be fitted to experimental data, which often correspond to normal operating conditions where the membrane is well humidified.

2.1.3. Concentration overpotential

The concentration overpotential arises due to gas transport limitations to the reaction. For detailed models where the through-plane gas concentrations are obtained, this concentration overpotential is simply accounted for by using gas concentrations in the catalyst layers for the calculation of the reversible potential and the activation overpotential. It is also possible to adopt this approach in 0D models, by calculating the gas concentrations in the catalyst layers from the channel concentrations with a quasi-steady state hypothesis for the gas transport in the porous layers, as done by some authors [34, 43, 44, 47, 71, 72]. In this case, the gas concentration in the catalyst layer is given by:

$$c_{CL} = c_{GC} - \frac{i}{4F} R_T \quad (8)$$

where R_T represents a global transport resistance, which can be obtained from the effective diffusivities in the porous layers and include the transport resistance at the channel-GDL interface. Most often, a specific term is used for the parametrization of the concentration overpotential [17, 20, 22, 30, 35, 38, 42, 54, 56, 60, 63, 64, 66–68, 70]. It generally involves a logarithmic function of the cell current and of a limit current, such as the one used by Schröder *et al.* [67] for the cathode:

$$\eta_{conc} = \left(1 + \frac{1}{\alpha_{ca}}\right) \frac{RT}{4F} \ln\left(1 - \frac{i}{i_{lim}}\right) \quad (9)$$

The limit current i_{lim} can be a constant or a function of the gas pressure, the temperature and sometimes an effective diffusivity in the porous layers, which allows to account for some flooding effects. The limit current can also be defined as the one for which the gas concentration is zero at the catalyst layer, which from equation 8 gives [77]:

$$i_{lim} = \frac{4F}{R_T} c_{GC} \quad (10)$$

In some cases, however, the concentration overpotential is not considered at all [18, 19, 21, 28, 29, 31, 32, 36, 48, 62]. This hypothesis can stand if the fuel cell operates at low to moderate current densities.

2.1.4. Other effects

Another effect considered by Goshtasbi *et al.* [61] and Futter *et al.* [50] is the impact of platinum oxide growth dynamics in the voltage of the fuel cell. They use an ordinary differential equation to model the evolution of the platinum oxide coverage and reduce the exchange current density for the cathode overpotential accordingly. Indeed, the formation of platinum oxide occurring for high operating voltages is reported to contribute to a large extent to recoverable performance loss in PEM fuel cells [78]. Further, it should be noticed that recent experimental evidence from Bernhard *et al.* [79] suggests that platinum oxide growth also add ohmic losses due to increased resistance to electronic transport in the oxide layers.

Electrochemical double-layer charging and discharging is neglected by most studies, as the characteristic time scales ($\approx 10^{-6}$ s) are orders of magnitude below those of mass and heat transport phenomena. Yet, a few models consider it, like those in [1, 18, 31, 49–51].

2.2. Catalyst layers

The anode and cathode catalyst layers are the places where electrochemical reactions occur. They combine carbon-supported catalyst nanoparticles and an ionomer binder and have a typical thickness of $1\ \mu\text{m}$ – $10\ \mu\text{m}$ [1]. In most studies, the catalyst layer is considered as infinitesimally thin, which means that there is no accumulation of species or energy in it and that the conditions in the CL-DM interface prevail over all the CL thickness. Of all the studies analyzed, only a few works [37, 58, 59, 61, 63] don't adopt this hypothesis. Yang *et al.* [58, 59] consider a single control volume for the CL, which also means that there can be accumulation of species or energy in it, although the transport of both across the through-plane direction in the CL is considered to be infinitely fast. Ritzberger *et al.* [63] do the same for the cathode CL, but consider the anode CL as infinitesimally thin. Goshtasbi *et al.* [61] and Zhou *et al.* [37] use respectively 4 and 30 control volumes to represent each CL, being able to solve transport equations in the through-plane direction across the CL. Xu *et al.* [69] consider one control volume for each CL for solving the transport equation for the membrane water content only, with the CL being considered infinitesimally thin for the other transport equations.

Some authors [50, 55, 61, 80] consider complex models to represent oxygen mass transport resistance in the cathode catalyst layer. While Goshtasbi *et al.* [61] and Futter *et al.* [50] use a homogeneous film model established by Hao *et al.* [80]. Chaudhary [33] and Han *et al.* [55] use an agglomerate model where platinum particles form an agglomerate coated with an ionomer film to compute the local rates of reaction in the anode and the cathode CL. Both models share the need for detailed data on the catalyst layer morphology, not necessarily available. But Weber *et al.* [14] notice that agglomerate models, although not corresponding entirely to reality, do provide better predictions.

Futter *et al.* [50] argue that in dry conditions the penetration depth of H^+ in the cathode CL is low due to low water content of the ionomer fraction, resulting in low utilization of the catalyst. Therefore, according to the authors, an appropriate model

of the through-plane transport in the CL is needed in such dry conditions. To account for this phenomena with only moderate computational cost, Goshtasbi *et al.* [61] calculate a cathode CL utilization factor, determined from the minimization of the sum of activation and proton transport losses in the CL.

It is important to note that the result of considering the CL as a single control volume or infinitesimally thin is the same if the transport equations for the different species are solved for the steady-state. The difference between both cases is the accumulation term, which is zero for the infinitesimally thin CL and non-zero for the single control volume CL, and which will have an impact only in dynamic responses.

2.3. Gas transport in the diffusion media

The diffusion media of a PEM fuel cell are composed of a gas diffusion layer and in some cases of a microporous layer. The function of those layers is to ensure the proper transport of reactant gases from the gas flow channels to the catalyst layers, while ensuring the electronic and thermal conduction between the catalyst layers and the bipolar plates, the evacuation of the produced water and the mechanical support and protection of the catalyst layers. The gas diffusion layers have a typical thickness around $200\ \mu\text{m}$, while the microporous layer have a typical thickness around $50\ \mu\text{m}$. The microporous layer has a finer structure than the GDL, positively impacting water management [1]. But from a modelling point of view, the GDL and MPL are generally treated essentially in the same way.

Concerning the transport of gases in the diffusion media, a number of studies consider it as infinitely fast [17, 26, 27, 31, 32, 35, 42, 48, 52, 65, 68–70], which is a valid hypothesis in most cases, since the characteristic time of the GDL is in the order of $1\ \text{ms}$ – $10\ \text{ms}$ [2]. That means that the concentrations are homogeneous across the DM and are the same at the DM-CL and DM-channel interfaces. All of those works also consider the CL as being infinitesimally thin. Several authors [11, 20, 43, 47, 61, 63, 67, 69] consider a steady-state Fickian diffusion across the DM. This allows to account for a transport resistance caused by the DM, but without any accumulation of gas species in the DM. Others consider one [58] or more [37, 39, 40] control volumes across the DM while using the Fick's law, therefore allowing for accumulation effects. In the case of Ziogou *et al.* [30], steady-state Fickian diffusion is considered for oxygen and hydrogen, but water vapor can accumulate in the DM control volume.

Several authors [19, 41, 46, 50] use the more complex Stefan-Maxwell diffusion. The work of Lindstrom and Wetton [81] indicates that Fickian diffusion can be a good approximation for the gas transport in the cathode DM when air is used as oxidant in the fuel cell. The same is not true for the anode DM if hydrogen is diluted in nitrogen, a condition that can be found with anode gas recirculation.

Only Chaudhary *et al.* [33] and Futter *et al.* [50] consider the hydraulic permeation of the gas phase in the through-plane direction across porous layers, which is modelled according to Darcy's law. Most authors neglect this hydraulic permeation arguing that the gas pressure gradient is negligible across the porous layer. Qin *et al.* [51] consider hydraulic permeation in

the in-plane direction for serpentine flow-fields by calculating the share of the flow going through the DM with 3D CFD simulations as is done in the work of Park and Li [82].

The case of water vapor is particular, as it may be coupled to liquid transport through phase-change. Zhou *et al.* [37] for instance only solve the transport equation for water vapor and not for other gases. In their steady-state model, Jiang *et al.* [11] compare the net water transfer flux across the membrane to the evaporation flux at the DM-channel interface to determine whether the water transport through the DM happens in the liquid or vapor form, in which case the Fick's law is applied.

It is also important to note that although several authors ignore gas transport phenomena across the diffusion media (and the CL), its impact on the cell voltage is most often still considered through a parametrization of the transport overpotential as explained in section 2.1.

Finally, the effective diffusivity in diffusion media such as the GDL is obtained by multiplying the bulk diffusivity by a correction factor to account for porosity and tortuosity effects. Most often, this factor consists in a power function of the medium porosity such as:

$$D^{eff} = D^{bulk} \varepsilon^{1.5} \quad (11)$$

or :

$$D^{eff} = D^{bulk} \left(\frac{\varepsilon - \varepsilon_p}{1 - \varepsilon_p} \right)^{0.785} \quad (12)$$

A discussion of the different expressions can be found in the review paper of Andersson *et al.* [8]. They conclude that some expressions which are used in the fuel cell modelling community may not be valid as they were obtained for porous media with different characteristics from those of fuel cell diffusion media, leading to an overestimation of the effective diffusion coefficients. Corrections to account for the saturation of the medium can also be applied if liquid water is present. Those corrections are discussed in section 2.6.

2.4. Liquid water and phase-change

The consideration of liquid water and phase-change is perhaps one of the most critical aspects for water management. Through-plane transport of liquid water in the porous layers is a complex issue and several approaches to handle (or avoid) it can be found in the literature. Some authors such as Striednig *et al.* [71] and Abdin *et al.* [43] consider that only water vapor exists in the stack. Liso *et al.* [46] consider that water in the liquid phase is finely dispersed in the gas phase, and no distinction is made between the two phases. The authors recognize that this can only be a valid assumption if the amount of excess liquid water is low. This is also the case for some other authors [27, 32, 52] although the hypothesis is not so explicit. In some works [17, 26, 64] the cathode and the anode sides are modelled as a single control volume each (infinitesimally thin GDL, MPL and CL) and therefore there is no liquid transport in the through plane direction, even though liquid water can accumulate in those control volumes. Damour *et al.* [31] does not consider the presence of liquid water, considering only the gas streams to be saturated with water vapor in order to compute

the membrane conductivity. The same hypothesis is adopted by Schultze and Horn [48]. Ritzberger *et al.* [63] consider that although liquid water may exist in a control volume (the CL or the channel), water transport between two control volumes can only happen under the gas phase. De Campo [54] considers that the water can accumulate in the gas channels through condensation, but be removed by convection with the same velocity as the gas phase. Wang and Chen [83] propose a non-dimensional Damkhöler number defined as the ratio between water production at the CL and water removed by vapor diffusion across the diffusion media to characterize the existence of two-phase flow in the diffusion media. A Damkhöler number close to zero indicates single-phase operation, while a value much greater than unity indicates two-phase conditions everywhere in the cathode. This non-dimensional number can then be used to evaluate the need for a two-phase model where liquid water transport is considered.

Liquid water transport is most often modelled using Darcy's law [11, 20, 33, 36, 37, 39, 40, 47, 58, 61, 67, 69, 70]. The liquid water flux is then written:

$$q_l = - \frac{\rho_l K_l^{eff}}{M_{H_2O} \mu_l} \frac{dp_c}{dx} \quad (13)$$

with the effective permeability calculated as $K_l^{eff} = K_{l,abs} K_{l,rel}$. The relative permeability $K_{l,rel}$ is modelled as a function of the water (and ice) saturation : $K_{l,rel} = s^n$ or $K_{l,rel} = s^n (1 - s_{ice})^n$. The exponent n can take prescribed values such as 5 [49, 61], 4 [11, 25, 37], 3 [20, 33, 34, 36, 47, 58, 69, 70], 2.5 [50] or even be fitted during model calibration [67]. Chaudhary *et al.* [33] add to equation 13 a term to account for the shear force exerted by the gas-phase velocity over liquid-phase, as they also consider the hydraulic permeation of the gas phase.

A closure relation between the capillary pressure and the water saturation completes equation 13:

$$p_c = \frac{\sigma_l \cos \theta_i}{(\varepsilon_i K_l)^{1/2}} J(s) \quad (14)$$

$$\frac{dp_c}{dx} = \frac{dp_c}{ds} \frac{ds}{dx} = \frac{\sigma_l \cos \theta_i}{(\varepsilon_i K_l)^{1/2}} \frac{dJ}{ds} \frac{ds}{dx} \quad (15)$$

The most commonly adopted parametrization for the so-called Leverett J-function $J(s)$ has been obtained by Udell [84] by fitting experimental data for sands from Leverett [85]:

$$J(s) = 1.417s - 2.120s^2 - 1.263s^3 \quad (16)$$

It is used by many authors [11, 20, 25, 34, 36, 37, 50, 58, 61, 69, 70] although its applicability has been questioned [1, 8] as it has been obtained for the water transport in soil materials. Alternatively, Schröder *et al.* [67] use a fitted function for a SGL10BA GDL taken from Gostick *et al.* [86] and Chaudhary *et al.* [33] a fitted function obtained by Kumbur *et al.* [87] for the SGL series. However, Jiao and Li [25] and more recently Vetter and Schumacher [12, 13] found that the J-function parametrization had little impact on the simulation results.

In the previous equations (13–16), some authors [20, 44, 67] use, instead of the actual saturation s , a reduced saturation defined as:

$$s_r = \begin{cases} \frac{s - s_{im}}{1 - s_{im}} & \text{if } 0 < s \leq 1 \\ 0 & \text{if } s = 0 \end{cases} \quad (17)$$

where s_{im} is the immobile water saturation level. s_{im} is considered equal to 0.08 in Schröder *et al.* [67]. According to Gerteisen *et al.* [24], immobile water saturation correspond to liquid water located in hydrophilic regions of the GDL. These authors assume $s_{im} = 0.2$ in the GDL and zero in the CL, a value also adopted by Goshtasbi *et al.* [44]. Gostick *et al.* [86] measured values between 0.04 and 0.13, depending on the GDL material.

The liquid water flux being calculated with equations 13–16, conservation equations can be written in several forms, especially depending on how the control volumes are discretized. In del Real *et al.* [20] the liquid water is considered to occupy uniformly the diffusion medium volume (with a infinitesimally thin CL). The saturation is considered zero at the channel so that the liquid water flux is defined as :

$$q_l = - \frac{\rho_l K_l^{eff}}{M_{H_2O} \mu_l} \frac{dp_c}{ds} \frac{s}{t_{GDL}} \quad (18)$$

A similar hypothesis is adopted by Strahl *et al.* [36]. We must note that $t_{GDL}/2$ should be used instead of t_{GDL} in equation 18 to be consistent with the cell-centered discretization used. Further, produced water is considered as a water vapor source in vapor form in the GDL, with the possibility of evaporation/condensation.

Yang *et al.* [58, 59], instead, use one control volume for each porous layer (CL, MPL, GDL) and a careful treatment of effective transport properties between two layers. Further they solve a partial differential equation for the liquid pressure, rather than for the liquid saturation. The liquid pressure continuity across the interface between two layers justifies this choice. The authors only use a water saturation conservation for the gas channel control volume, considering convective liquid water transport. This convective transport is calculated from the liquid velocity, obtained by applying a slip ratio to the gas velocity. In [59] the liquid velocity is considered to be the same as the water vapor velocity, although this hypothesis is not explicit in [58]. Evaporation/condensation are also considered as source-terms in the transport equations both in the porous layers and the gas channel. A similar approach is adopted by Tang *et al.* [49, 88]. But these authors use a modification of the Lockhart-Martinelli correlation to compute the liquid-gas slip ratio, instead of assuming it equal to unity. Gong *et al.* [70] solve the same equations as Yang *et al.* [58] but instead of one control volume for each porous layer, they use a single control volume to represent the combination of CL, MPL and GDL and consider the water saturation to be homogeneous across those layers.

Salva *et al.* [47] consider one control volume for each layer (CL, MPL, GDL) as in Yang *et al.* [58, 59], but solve the transport equation for the steady-state and assume equilibrium between liquid and vapor phases in each layer, with infinitely fast

evaporation and condensation. While the infinitely fast evaporation corresponding to a local equilibrium of liquid and vapor phases is assumed by a number of authors, it can bring numerical difficulties due to the discontinuity arising from water condensation. Strategies to smooth the transition between unsaturated and supersaturated conditions are proposed by Chen *et al.* [60] and Ritzberger *et al.* [63].

Kang [39] solves a partial differential equation for the total water transport in the GDL, which is discretized with four control-volumes in the through-plane direction. Evaporation and condensation are assumed to happen infinitely fast and the resulting saturation is used to calculate a liquid water flux between two adjacent control volumes, included in the total water transport equation. The CL is supposed to be infinitesimally thin. The authors say that the presence of liquid water in the gas channels is neglected, but it is not clear how this assumption is considered in the model equations.

Schröder *et al.* [67] propose an original approach. The authors solve the mass conservation equation to obtain the total amount of water accumulated in the reference volume (gas channel + GDL pores). From that, the authors calculate the relative humidity in the reference volume. The water flow from the CL to the gas channel is considered to be equal to the sum of water produced from the reaction and transported across the membrane. If the relative humidity in the reference volume is equal to 100%, all the water flow from the CL to the gas channel is considered to be in liquid form. The authors then solve a 1D steady-state transport equation for liquid water in order to obtain the reduced water saturation profile $s_r(x)$ across the GDL. An average reduced saturation over the GDL thickness is then obtained. This average value is finally scaled with a fitted parameter to mimic along-the-channel effects.

Goshtasbi *et al.* [61] and Zhou *et al.* [37] solve the 1D partial differential equation with more than one control volume for each porous layer. Goshtasbi *et al.* use 20 for each GDL, 4 for each MPL and 4 for each CL, but vapor and liquid equations are decoupled. First the vapor concentrations are obtained through a quasi-steady approximation. These vapor concentrations allow for the calculation of phase-change source terms for the transient liquid transport equation. Vapor fluxes are updated to account for phase-change. An average saturation in the GDL is used to modify the gas diffusivities in turn. Readers should refer to [44] for more details on this method. Zhou *et al.* use 30 for each GDL and 20 for each CL and also decouples the liquid transport from the vapor transport, which is solved with a single control volume for the GDL and a single control volume for the CL.

Finally, Xu *et al.* [69] use analytical solutions for the transport of liquid water across the GDL obtained by Hu *et al.* [89] from the integration of 1D through-plane transport equations for three different regimes: unsaturated vapor throughout the GDL, saturated vapor throughout the GDL and a mixed regime where a saturation front exists. A similar approach is adopted by Jiang *et al.* [11], where a switching function is used to determine whether the water is transported as liquid or vapor in the porous layers.

It should be noted that many papers use as boundary con-

dition between the GDL and the gas channel a fixed small (or zero) saturation, since any liquid water would be quickly removed by the gas stream [11, 30, 33, 37]. The exceptions are works of Jiao's group [58, 59, 70] where a saturation conservation equation is solved for the channel, Gerteisen *et al.* [24] where the authors impose a liquid water flux proportional to the gas flow rate and the square of the difference between the saturation s and its immobile part $(s - s_{im})^2$. On the membrane-CL interface, most papers use a zero-flux boundary condition. Exceptions are the works of Tang *et al.* [49, 88] that considers the possibility of hydraulic permeation of liquid water from the CL into the ionomer and the one of Chaudhary *et al.* [33] that considers separate liquid and vapor water absorption/desorption by the membrane.

2.5. Heat transfer

In fuel cells, heat is released by electrochemical reactions and ohmic resistances. Water condensation or evaporation constitute a heat source as well. Most heat is released in the MEA, due to entropic and irreversible reaction heat in the CL and protonic resistance in the membrane and the ionomer phase of the CL [90]. In liquid-cooled or air-cooled fuel cells, the excess heat is evacuated by the coolant flowing in channels in the bipolar plates. Due to water phase-change and thermal gradients, water and heat transport are tightly coupled, so that heat transfer is key for both water and thermal management.

The majority of system-level studies consider a homogeneous stack temperature, identical in all cells, across all the cell layers and across all the cell surface [17, 20, 22, 26, 27, 31, 32, 35, 36, 42, 43, 46, 48, 52, 54, 62, 63, 65, 66, 68]. In their work, Schröder *et al.* [67] also consider a homogeneous stack temperature, but with a different temperature for the gas in the cathode gas flow channels. In some works as Hoeflinger and Hofmann [62] or Abdin *et al.* [43], the temperature is an input parameter of the model and considered to be constant. Most often [22, 35, 36, 54, 68], however, a single energy balance equation is solved, with the general form:

$$C_{st} \frac{dT_{st}}{dt} = \sum (\dot{m}h)_{in} - \sum (\dot{m}h)_{out} - P_{el} - \dot{Q}_{cool} - \dot{Q}_{amb} \quad (19)$$

It should be noticed that this hypotheses is less valid for short stacks with few cells (where heat losses through the end plates might be significant), for high surface area cells where temperature differences across the cell surface might be significant and, above all, for high current densities where the amount of heat released is high and thermal gradients are strong. Nandjou *et al.* [10] put in evidence temperature differences of up to 10 °C at 0.8 A cm⁻² for a cell with an active area of 220 cm². Wang *et al.* [91] also indicates that temperature differences across the GDL can reach 5 °C–10 °C. Due to the steep relation between temperature and saturation pressure of water, small changes of temperature may lead to strong variations of relative humidity. For instance, 100 % RH at 75 °C gives only 81 % RH at 80 °C or 67 % RH at 85 °C if the water vapor pressure is kept constant. This highlights the fact that only small changes in temperature can have significant impact for water management.

Tang *et al.* [49, 88] treats the solid and gas with different temperatures in the CL and the GDL, although the fluid and solid domains are supposed to be in thermal equilibrium in the membrane. In the CL and the GDL, the condensing liquid film is assumed to be at the same temperature as the solid.

Salva *et al.* [47] on the other hand, considers the gas-phase to be in equilibrium with the solid layer they are flowing in, each of these layers (membrane, CL, MPL, GDL, BPL) having an homogeneous temperature. Heat is transferred between the layers by conduction, characterised by heat transfer resistances. An originality of the model is that each layer can lose heat to the environment at its perimeter. Reaction heat is considered to be fully released in the cathode CL. The authors don't mention any kind of active cooling, but it could be easily accounted for in the equations, as is done in Yang *et al.* [58]. Instead, they consider the temperature of the cathode BP as known and use it as an input parameter. The equation for the cathode GDL heat balance, for instance, is written:

$$\frac{T_{GDL} - T_{CL}}{R_{CL-GDL}} + \frac{T_{GDL} - T_{BP}}{R_{GDL-BP}} + A_{lat,GDL}h(T_{GDL} - T_{amb}) = 0 \quad (20)$$

It should be noticed that the authors' approach implies that heat capacities of gases and liquid water inside the cell is negligible, and that equations are solved in steady-state. Further, they don't seem to account for the latent heat released by water condensation in the energy balances.

Yang *et al.* [58, 59] adopt an approach similar to Salva *et al.* for the through-plane discretization of the heat equation, but consider transient effects with a forward Euler discretization. For the cathode GDL, it gives:

$$T_{GDL}^t = T_{GDL}^{t-\Delta t} + \frac{\Delta t}{(\rho C_p)_{GDL}} \left(\frac{T_{GDL} - T_{CL}}{R_{CL-GDL}} + \frac{T_{GDL} - T_{BP}}{R_{GDL-BP}} + S_T \right) \quad (21)$$

where S_T is the heat source term which includes different terms depending on the layer. The thermal resistances R_{i-j} between layers i and j are calculated by using effective thermal conductivity values which account for the fractions of the different phases in each layer (gas, liquid and solid) [59]. Heat can be also exchanged between different cells of the stack, which are considered individually. The same approach is adopted by Zhou *et al.* [37] or Chaudhary *et al.* [33], although these authors use a more detailed discretization in the through-plane direction.

Gosthasbi *et al.* [61] and Kang [39] also adopt this approach but with some differences. Gosthasbi *et al.* [61] take the gas channel temperatures as boundary condition. The authors suppose the gas channel temperature in the k -th channel segment to be equal to the cooling fluid temperature in that segment, which in turn is given by a linear dependence on the local current density i_k :

$$T_{cool,k} = T_{cool,in} + \frac{\sum_{j=1}^k i_j}{\sum_{j=1}^{N_{seg}} i_j} \Delta T_{cool} \quad (22)$$

Kang [39] considers also convection heat transfer in the gas diffusion layer.

It should be noted that a recent numerical study by Sauer-moser *et al.* [92] indicates that Peltier and Dufour effects impact significantly the heat fluxes in the cell. As far as we know, these effects have not been taken into account by any system-level study so far.

2.6. Flooding effects in the porous layers

The main effect of the presence of liquid water (or ice) in the electrodes and porous layers is the blockage of the reactant's access to the catalytic sites. It can be taken into account in different ways. Many studies [11, 25, 33, 34, 37, 44, 47, 50, 53, 55, 57–59, 61, 67, 69, 70] use an effective diffusivity to calculate gas transport which includes the effect of the liquid water saturation in the wet porous layers:

$$D_{k,wet}^{eff} = (1 - s)^{n_s} D_{k,dry}^{eff} \quad (23)$$

with n_s , usually varying between 1 and 3 [2, 15]. The ice volume fraction can be added to the liquid saturation when pertinent. This reduction in the effective diffusivity will increase the gas transport resistance and thus impact the concentration overpotential of the cell (see section 2.1.3). In some works [24, 50, 55, 61] where agglomerate or film models are used for the catalyst layer, the liquid saturation in the will add an oxygen transport resistance due to the presence of a liquid film covering the ionomer film. Other authors [20, 36, 37, 39, 40, 49] consider the effect of liquid water through a reduction in the effective cell active area proportional to the water saturation:

$$A_{cell}^{eff} = (1 - s)A_{cell} \quad (24)$$

Strahl *et al.* [36] adopt an original approach by considering that the water saturation of the cathode catalyst layer will increase the active area until an optimum saturation value is attained, after which the active area will remain constant:

$$A_{cell}^{eff} = A_{opt} [\exp(k_s s) - 1], \quad 0 < s < s_{opt} \quad (25)$$

where A_{opt} and k_s are both fitting parameters. The same authors Strahl and Costa-Castelló [93] propose the following equation in a latter work:

$$A_{cell}^{eff} = A_{opt} \left(1 - \frac{s_{opt} - s}{s_{opt}} \right)^{1/3} \quad (26)$$

with the fitting parameter s_{opt} . As we will see in section 4, adopting this relation between active area and liquid saturation allow the model to better fit transient voltage data. The increase of the active area with liquid saturation is in line with experimental observations reported by Padgett *et al.* [94], where platinum utilization increases with the relative humidity for porous support materials. The authors argue that condensed in water allows the utilization of platinum catalyst present in pores that are too small for the ionomer to be in. Finally, it is important to notice that the works of Strahl *et al.* [36, 93] concern open-cathode fuel cells where the cathode stoichiometry is rather high (> 20).

2.7. Membrane mass transport

Water transport across the PFSA membrane is essential to water management, as it will define water content and humidity levels across the MEA. While readers should refer to the work of Kusoglu and Weber [95] for a comprehensive review on physical phenomena occurring in the membrane, the review of Dickinson and Smith [96] presents very well approaches for the continuum modelling of water fluxes across the membrane and the CL ionomer. Most often, system-level studies adopt the Springer membrane model [74] where the water flux in the membrane is considered as the sum of a Fickian diffusion term and electro-osmotic drag term [96]:

$$q_w = -D_\lambda c_f \nabla \lambda + \xi \frac{i}{F} \quad (27)$$

The parameters D_λ and ξ depend on the material as well as on the temperature and the membrane water content, with several parameterisations available in the literature. An alternative approach is to use the model proposed by Weber and Newman [76, 97], as Futter *et al.* [50] do. Sorption isotherms are also available and give the equilibrium water content λ_{eq} as a function of the temperature and the water activity. These sorption isotherms have generally been obtained for Nafion 1100 and Dickinson and Smith [96] caution against their use for other materials even in the Nafion family. Such use is nevertheless a common practice due to a lack of data for specific materials. Authors such as Goshtasbi *et al.* [61] and Del Real *et al.* [20] try to go around the problem by fitting a correction factor for the water diffusion coefficient, while Abdin *et al.* [43] use a constant water diffusivity coefficient. The reader should refer to the works of Dickinson and Smith [96] and Vetter and Schumacher [12] for discussions and comparisons of the different parameterisations available for the membrane water diffusivity, electro-osmotic drag coefficient and soption isotherms.

System-level studies have proposed different approaches to calculate the water flux across the membrane and the membrane water content. The simplest one is to consider that the membrane has a constant water content, often corresponding to well-humidified conditions [31, 42, 48, 54, 65, 68]. Strahl *et al.* [36] go further and neglect the water flux across the membrane, arguing that electro-osmotic and diffusive fluxes have the same order of magnitude and therefore cancel each other for the low current densities where their open-cathode fuel cell stack operates. A popular alternative consists in considering that the membrane-CL interfaces are in equilibrium with water contents λ_{ca} and λ_{an} (calculated from the water activities in each CL) and to consider the membrane water content to be the average value as in the work of Prukushpan *et al.* [17]:

$$\lambda_{memb} = (\lambda_{ca} + \lambda_{an})/2 \quad (28)$$

with the gradient $\nabla \lambda$ calculated as:

$$\nabla \lambda \approx (\lambda_{ca} - \lambda_{an})/t_{memb} \quad (29)$$

Similarly, some authors [32, 38, 67] adopt a linear water content profile across the membrane:

$$\lambda(x) \approx \lambda_{an} + x \times (\lambda_{ca} - \lambda_{an})/t_{memb} \quad (30)$$

and use it to obtain average values of D_λ and ξ . Del Real *et al.* [20] and Ziogou *et al.* [30] use instead the anode water content to calculate the diffusivity across the membrane and the electro-osmotic coefficient. Oppositely, Huisseune *et al.* [21] consider the membrane water content as being constant and equal to the cathode water content λ_{ca} . A more common approach [29, 35, 47, 54] is to consider a membrane water content corresponding to the equilibrium water content for an average water activity given by:

$$\lambda_{memb} = \lambda_{eq} \left(\frac{a_{ca} + a_{an}}{2} \right) \quad (31)$$

These approaches do not consider the possibility of water accumulation in the membrane and no conservation equation is solved for a membrane control volume in the membrane. That means that they cannot reproduce the dynamics of membrane sorption.

In an attempt to describe the dynamics of water accumulation in the membrane, Ritzberger *et al.* [63] consider the membrane water activity to follow the average $(a_{ca} + a_{an})/2$ as in the work of Salva *et al.*, but with a time constant τ_{memb} :

$$\dot{a}_{memb} = -\frac{1}{\tau_{memb}} \left(a_{memb} + \frac{a_{ca} + a_{an}}{2} \right) \quad (32)$$

Goshtasbi *et al.* [44, 61] consider hydraulic liquid water and thermo-osmotic in addition to electro-osmotic and Fickian diffusion, yielding:

$$q_w = -D_\lambda c_f \nabla \lambda + \xi \frac{i}{F} - \frac{K_l}{\mu_l M_{H_2O}} \nabla p_l + D_T \nabla T \quad (33)$$

Hydraulic permeation is also accounted for in a few other works [11, 21, 56]. Dickinson and Smith [96] mention that hydraulic permeation might play a role only for liquid-equilibrated conditions.

In terms of membrane water conservation, Goshtasbi *et al.* [44, 61] solve a conservation equation for three control volumes corresponding to the whole membrane thickness, and for the ionomer in each of the catalyst layers. This is also done by Yang *et al.* [58, 59] and Xu *et al.* [69]. Kang [39] consider a single control volume for the membrane thickness, but no conservation equation for the water content in the CL ionomer, with diffusion fluxes calculated assuming equilibrium water contents in the membrane-CL interfaces. Zhou *et al.* [37] however considers 50 control volume for the through-plane discretization of the membrane.

Only some authors [37, 46, 58, 59, 61, 69] also consider the non-equilibrium dynamics of water absorption (or desorption) into the ionomer, with the absorption flux q_{abs} written:

$$q_{abs} = k_{abs} c_f (\lambda_{eq} - \lambda) \quad (34)$$

In particular, Liso *et al.* [46] show with steady-state water balance measurements that considering such non-equilibrium conditions lead to better prediction of membrane water fluxes, while considering equilibrium water content at the membrane-CL interfaces yields overestimated membrane water fluxes.

They used a Nafion 112 membrane. Majsztzik *et al.* [98] also provide evidence of the importance of the interfacial transport resistance for the membrane sorption, specially for thin membranes. Xu *et al.* [69] adopt an weighted average of the absorption/desorption rate constants for vapor and liquid water to account for faster kinetics when the membrane is in contact with liquid water, with the weighting factor depending on both the ionomer water content and the water activity. Dickinson and Smith [96] recommend the use of the water activity difference between the membrane and the gas phase as the driving force, rather than the membrane water content as in equation 34:

$$q_{abs} = k_{abs} (a_{ca/an} - a_{memb}) \quad (35)$$

Further, they mention that there is no consensus on whether an active electro-osmotic water uptake should be considered, yielding:

$$q_{abs} = -\xi \frac{i}{F} + k_{abs} (a_{ca} - a_{memb}) \quad (36)$$

$$q_{abs} = \xi \frac{i}{F} + k_{abs} (a_{an} - a_{memb}) \quad (37)$$

One aspect that is often neglected in the modelling of membrane water absorption/desorption dynamics is the so-called Schröder's paradox, consisting in different membrane water uptakes depending on if the membrane is in contact with liquid water or saturated water vapor [2, 96]. Chaudhary *et al.* [33] evaluated two approaches to account for Schröder's paradox, both considering individual contributions for membrane water absorption/desorption from vapor and liquid phases, with membrane water desorption occurring only in the liquid phase. In a first approach, different membrane water equilibrium concentrations are considered depending on the water phase, liquid or vapor. In the second approach, a single value of the membrane water equilibrium concentration is considered for both phases. The authors show that the first approach gives better results when the anode and cathode inlet gases are fully humidified (RH = 100%), which is probably link to the presence of liquid water. Futter *et al.* [50] account for the Schröder's paradox by using in the membrane transport equations an expression for the chemical potential of water that depends on the local water saturation.

Another aspect that many authors neglect is the fact that ionomer thin-films in the catalyst layer might behave significantly differently from the bulk material in the membrane, as deeply discussed by Weber *et al.* [14]. Differences include lower equilibrium water content and conductivity or higher activation energy for the thin-films as compared to the bulk ionomer. It is remarkable that no study takes into account these effects.

The permeation across the membrane of species other than water, namely N_2 , O_2 and H_2 , is most often neglected. Yang *et al.* [58, 59] consider the crossover of nitrogen only, with a correction factor for the crossover rate to match experimental data. Ritzberger *et al.* [63] also consider only the crossover of nitrogen. Differently, Futter *et al.* [50] consider the transport of O_2 and H_2 across the membrane. Among the models discussed in

this work, the ones of Goshtasbi *et al.* [61], Tang *et al.* [49] and Chen *et al.* [60] are the only taking into account the crossover N_2 , O_2 and H_2 .

2.8. Gas flow channels

Most studies consider a single control volume to represent the gas flow channel [17, 20, 27, 29, 31, 35, 52, 54, 63, 68], which is perhaps the simplest approach. In this case, the mass conservation equation for each gas species is written in the general form:

$$\frac{dm_{k,GC}}{dt} = \dot{m}_{k,in} - \dot{m}_{k,out} + S_k \quad (38)$$

This equation is often combined with linear nozzle equations to determine the inlet and outlet mass flow rates from the pressure difference between the gas flow channel control volume and upstream or downstream pressures [17, 52, 63]. The mass source term S_k can include any transport of species from the channel to the GDL. Schultze and Horn [48] adopt a similar model but use it to derive a first-order transfer function to represent the cathode gas flow channel. The time constant of this transfer function is fitted to experimental data.

Other authors use a one-dimensional discretization along the channel direction to capture heterogeneity over the cell surface. Goshtasbi *et al.* [61] use 12 or 27 control volumes along the channels, depending on the channel length, as the authors noticed that control volume lengths of more than 1 cm lead to numerical issues. The authors consider that no species can accumulate in the channel so that for each segment i the following equality holds:

$$\dot{m}_{k,out}^i = \dot{m}_{k,in}^i + S_k^i \quad (39)$$

Further, the authors use an iterative procedure to simulate counter-flow configurations. Yang *et al.* [58] adopt a similar approach to the one of Goshtasbi *et al.* [61], combining an explicit time discretization and a first-order upwind discretization along the channel, so that the total mass flow at the outlet of a channel segment can be calculated from the inlet mass flow and other mass sources at the previous time step:

$$\dot{m}_{out}^{i,t+\Delta t} = \dot{m}_{in}^{i,t} - \sum_k S_k^{i,t} \quad (40)$$

as explained in Wang *et al.* [53]. The use of an explicit time discretization allows the consideration of counter-flow configurations, but at the expense of small time steps (of the order of 10^{-6} s). Interestingly, Yang *et al.* [58] give the results of a convergence study showing that the three nodes along the channel are sufficient to keep the relative error within $\pm 0.5\%$ as compared to ten nodes for the outlet gas velocity, the water saturation in the CL and the output power of the stack. With a single node, the relative error remains within $\pm 1\%$ for the two latter parameters, but attain near 6% for the outlet gas velocity. Kang [39] adopts a 2D discretization along the channel with 20 control volumes, but only convection in the flow direction and through-plane transport in the porous layers are considered. The only 2D transport considered is the heat conduction in the bipolar plates. Pressure drop along the channels is calculated

from the friction factor, but it is not clear how outlet flow rates are calculated for each control volume.

Schröder *et al.* [67] adopt a pragmatic approach to deal with the problem of along-the-channel heterogeneity. The total volume of fluid leaving each gas channel is calculated for steady-state conditions, while water is allowed to dynamically accumulate in the cathode or the anode. Cathode oxygen mole fraction and the cathode pressure are the average between the inlet and outlet values. However, the cathode fluid temperature is calculated from a fitted linear combination of inlet and outlet temperatures. An effective relative humidity is also calculated by multiplying the cathode relative humidity by a fitted coefficient. The authors argue that this allows to take into account the non-linear dependence of the ionomer's ohmic resistance on the relative humidity. It should be noted that some authors such as Lazar *et al.* [56] use a logarithmic average to account for non-homogeneous distribution along the gas flow channel, but without any justification.

Falcão *et al.* [23] adopt another approach by considering that the gaseous species concentrations at the channel outlet are equal to the concentrations at the GDL-channel interface, and that the gas volume flow rate is constant along the channel. Their model assuming steady-state operation, balance equations can thus be written such as, for instance, the one for the oxygen on the cathode side:

$$\frac{i}{4F} = \frac{\dot{Q}_{ca,in}}{N_{cells}A_{cell}} (c_{O_2,GC}^{in} - c_{O_2,GC-GDL}) \quad (41)$$

If all the other parameters are known, that allows one to obtain the boundary condition of the through-plane transport, $c_{O_2,GC-GDL}$. Salva *et al.* [47] also adopt this approach.

One important aspect in the modelling of the gas flow channels is the liquid water transport along the channel. Several authors [20, 26, 35, 40, 42, 48, 63] consider that only water vapor is transported along the channel and leaves the stack. In particular, Zhao *et al.* [42] consider that the cathode and anode outlet gases are fully saturated (RH = 100%) with no liquid water. Schultze and Horn [48] also adopt this hypothesis for the cathode, but don't include the anode channel in their model. Conversely, Qin *et al.* [51] suppose that the anode outlet gas is fully saturated with no liquid water, instead of the cathode. Zhou *et al.* [37] and Strahl *et al.* [36] consider that the water saturation is zero in the channel arguing that any liquid water is quickly removed by the gas flow. Del Real *et al.* [20] allow for liquid water removal during anode purge events, where they consider that all liquid water is removed from the anode. Some authors [32, 46, 61, 67] assume that liquid water is present in a dispersed phase in the gas flow channels and use a total water molar flow in the calculations, representing the sum of liquid and vapour water in the channel. Yang *et al.* [58] use a fixed velocity ratio to obtain the liquid phase velocity from the gas velocity in the channels. The value of the velocity ratio is not mentioned, but in a previous work of the same group [53] this velocity ratio is equal to one, indicating that a dispersed phase is also assumed. A velocity ratio equal to one is also adopted by De Campo [54], while Tang *et al.* [49, 88] use a modification of the Lockhart-Martinelli correlation to compute the liquid-gas

velocity ratio. In the analytical solutions for the through-plane water transport of Hu *et al.* [89] used in the model of Xu *et al.* [69], an interfacial drag assumption is adopted, with the liquid velocity given by:

$$v_l = v_g \frac{s_{GC}^3}{(1 - s_{GC})^3} \frac{\mu_g}{\mu_l} \quad (42)$$

Alternatively, Schultze and Horn [29] and Fly [38] consider the mass flow rate of liquid water leaving the cathode to be proportional to the gas mass flow rate. While Schultze and Horn don't mention which value they use as a proportionality constant, Fly fixes an arbitrary value of 2.

Finally, it is important to mention that a few authors [11, 34, 40, 58, 61] consider a mass transfer resistance between the channel gas flow and the GDL by using Sherwood number correlations, usually valid for fully developed laminar flow, but most neglect it. For two-phase conditions where droplets or films might be present in the channel, Sherwood number correlations are provided by Koz and Kandlikar [99–101].

2.9. Cell and stack heterogeneity

Operation conditions are not homogeneous over the active area of a fuel cell, as evidenced by the work of Miao *et al.* [102]. These conditions can also differ between different cells of a stack, with for instance temperature variations across the stack due to heat losses at the end plates. However, modelling those heterogeneous conditions require a level of spatial detail that most authors choose to neglect. Some attempts to consider them in a computationally efficient way have been made, nevertheless.

A first approach to consider heterogeneous conditions over the cell surface area is to use some kind of 1D+1D model, where in addition to the solution of the through-plane 1D transport equations, a 1D discretization along the channel direction is adopted, as described in section 2.8. Kang [40] is even able to account for some 2D effects over the cell active area for a serpentine flow field with their quasi-3D modelling. A serpentine flow field can also be modelled by the flow network model proposed by Qin *et al.* [51] But discretization along the channel is not enough to take into account the effect of the bipolar plate land area, where the plate is in contact with the GDL. Gosh-tasbi *et al.* [61] adopt a bi-domain approach, initially proposed by Zaglio *et al.* [103]. This approach is based on solving the through plane equations for two different domains: one under the channel and one under the land, with respective effective transport lengths and boundary conditions. It is schematized in figure 3. The effective transport length takes into account geometrical lengths but also anisotropy in the transport properties of materials. Schröder *et al.* [67] and Tang *et al.* [49] use a conformal mapping to calculate an effective length for each layer, as proposed by Weber [104]. In a simpler approach, Yang *et al.* [58] take the channel-land heterogeneity by considering only the channel area in the channel-GDL interface. None of the other works reviewed here consider channel-land heterogeneity.

In what concerns stack heterogeneity, all works except the ones of Zhou *et al.* [37] and Yang *et al.* [58] consider all the cells to operate identically, with the same conditions. Being so, the solution for a single cell is obtained and the resulting voltage and flow rates are multiplied by the number of cells in the stack to obtain results for the stack. Zhou *et al.* and later Yang *et al.* instead consider each cell individually, with heat exchange between adjacent cells and heat losses to the environment for the two end cells.

3. Modelling auxiliary components

The fuel cell stack model is at the heart of any fuel cell system modelling effort. However, having appropriate models of the different auxiliary components in the cathode, anode and cooling loops is almost as important for system-level studies. They allow to correctly assess the operating conditions to which the stack is subject in case of variable load or environmental conditions, estimate the system efficiency and evaluate the water and heat balances. In this section we review the modelling approaches adopted in the fuel cell modelling literature to account for some important components in fuel cell system studies.

3.1. Air compressor

The air compressor is a key element of the fuel cell system as it allows to increase the air pressure in the cathode, thereby improving the efficiency of the fuel cell stack. Several authors [17, 19, 27, 52, 54, 55, 58, 66] model the compressor by considering its dynamics, including a momentum conservation equation for the motor shaft and an equation for the dynamics of the DC motor current depending on the applied voltage. They generally determine the mass flow rate from the rotation speed and the pressure ratio with the help of a compressor map, that can be obtained experimentally or from supplier data and fitted to non-linear functions [17, 54, 58]. Some authors [40, 67, 68, 72] neglect the dynamics of the compressor and use only a static model, with the mass flow rate being given by the required air stoichiometry and stack current. Others [38, 63] consider that the mass flow rate follows the required mass flow rate with a first-order transfer function and a fixed time constant. The compressor isentropic efficiency can be obtained from the compressor map [40, 69] or considered as a constant [34, 38, 67, 68]. In addition to the compressor isentropic efficiency, mechanical transmission, DC motor and power converter efficiencies can also be considered [67, 72]. It is important to note that the compressor isentropic efficiency will have a significant impact on the air temperature at the outlet of the compressor. In Hoeflinger and Hofmann [62], the compressor pressure ratio and power consumption are fitted to non-linear functions of the mass flow rate and of the voltage applied to the air throttle valve placed downstream the cathode outlet. A review on different type of compressors and their application in fuel cell systems can be found in [105], which also includes a short review on the mathematical modelling of air compressors.

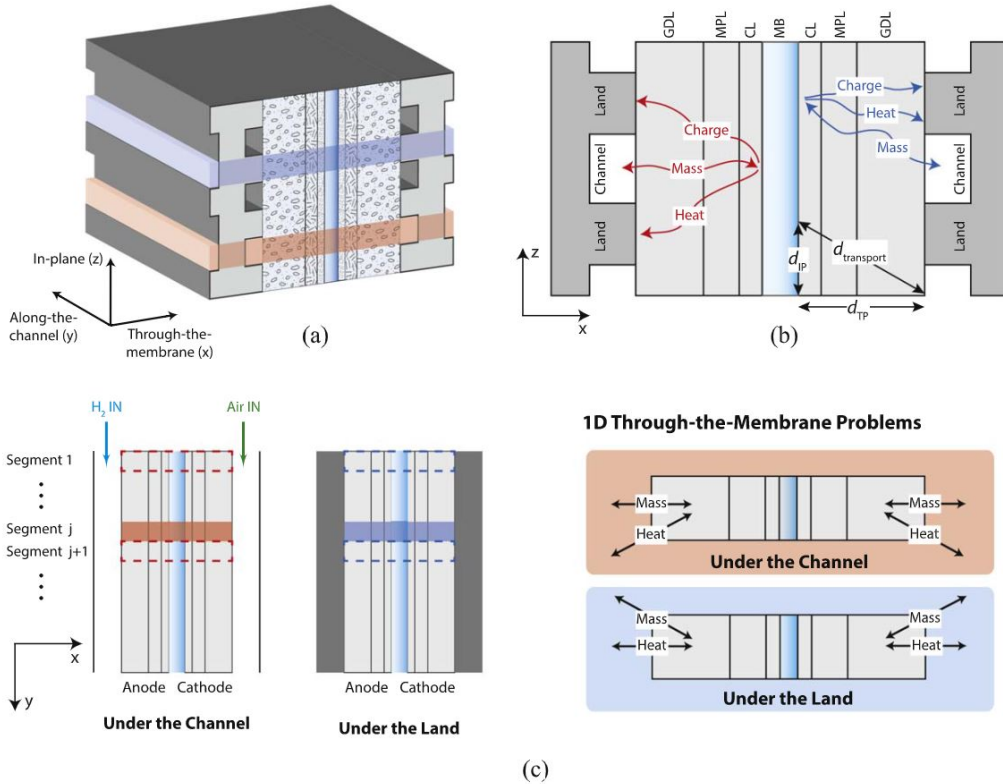


Fig. 3. Schematics of the bi-domain approach used by Goshtasbi *et al.* [61] to represent channel-land heterogeneity. (Reproduced from Goshtasbi *et al.* [61]).

3.2. Air humidifier

The air humidifier ensures that the cathode air is sufficiently humid to avoid the dehydration of the membrane. Most often, membrane humidifiers are used in fuel cell applications and they are sometimes included in system models. Yang *et al.* [58] use a plane membrane humidifier model analogous to their fuel cell model, but with a single control volume along the channel. This model is validated against water vapor transfer rate measurements for two dry side inlet temperatures (50 °C and 60 °C). To our knowledge, it is the only model that takes into account the dynamics of the membrane water content, although it is validated against steady-state measurements only. Tang *et al.* [88] and Kang and Min [40] also adopt a humidifier model analogous to their respective fuel cell mode, but with more control volumes along the channel, as schematized in figure 4. Kim *et al.* [34] and Fu *et al.* [66] use a 0D model for the membrane humidifier accounting for heat and water transport across the membrane. A simpler approach adopted for instance by some authors [17, 20, 31, 35, 55, 63] is to consider the air "ideally humidified" in the fuel cell inlet, thus avoiding any modelling of the membrane humidifier. The same is done by Schröder *et al.* [67] but they consider the pressure drop of the membrane humidifier in their calculations. Fly [38] uses an iterative method to calculate water and heat transfer in the membrane humidifier given a target relative humidity at the cathode inlet. De Campo [54] models an isothermal water injection humidifier by assuming that the dry gas partial pressure remain constant. Xu *et al.* [69] use an humidifier map providing the dew point temperature at the outlet from the dry air mass flow rate and

temperature. Other membrane humidifier models can be found in dedicated works, which propose steady-state or dynamic 0D [106] or 1D models [107–109], as well as models based on the NTU-effectiveness method [110, 111] or on experimentally obtained maps [112].

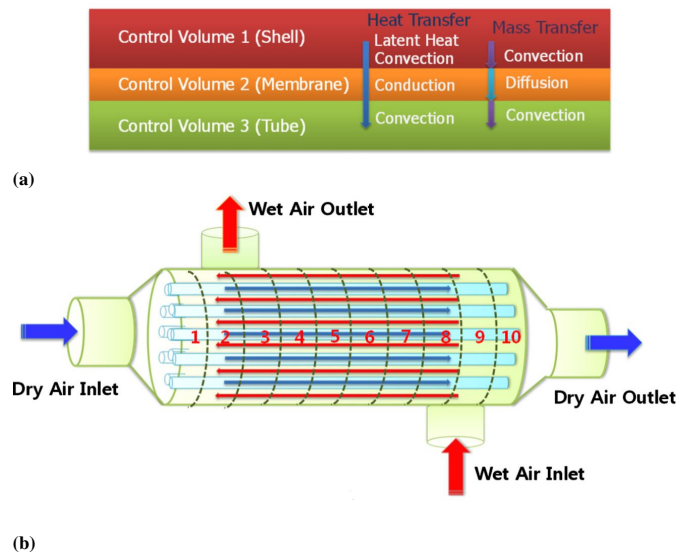


Fig. 4. Schematics of the 1D+1D shell-tube membrane humidifier model used by Kang *et al.* [40]. (Reproduced from Kang *et al.* [40] with permission from Elsevier).

3.3. Anode recirculation

Anode recirculation is generally used to allow for a high hydrogen stoichiometry without increasing hydrogen waste. Anode recirculation is implemented with a hydrogen mechanical pump, an ejector or an electrochemical pump, plus a gas-water separator [113]. Karnik *et al.* [26] and Bao *et al.* [19], calculate the ejector primary and secondary inlets from supply and return manifold pressures and temperatures. Yang *et al.* [58] model an electrochemical hydrogen pump used to hydrogen recirculation, with a model analogous to the one used for the fuel cell or the membrane humidifier. A simpler approach is adopted by Ritzberger *et al.* [63] and Liso *et al.* [35] who assume that the recirculation mass flow rate is known. In order to avoid the modelling of the anode recirculation loop, De Campo [54] used measurements of the anode inlet and outlet pressures and considered that the anode gas was saturated with water vapor in order to calculate the hydrogen partial pressure.

3.4. Cooling loop

In the case of liquid-cooled PEM fuel cells, the cooling loop ensures that the waste heat is evacuated from the fuel cell system. It generally consists of a coolant tank, a coolant pump and a radiator heat exchanger, often with a bypass [90]. Modelling the cooling loop allows to better account for the dynamics of the cooling fluid inlet temperature and, as a consequence, of the fuel cell stack temperature. Several authors [38, 58, 114] adopt NTU-based effectiveness models for the heat exchangers, while neglecting the heat capacity of the cooling fluid in the circuit. Schultz and Horn [48] also use a NTU-based method but instead take into account the heat capacity of the coolant fluid. Kang *et al.* [40] and Tang *et al.* [88] adopt 1D radiator models with respectively five and four control volumes in the flow direction. Wang *et al.* [65] adopt a similar model but with a single control volume in the flow direction, while accounting for the thermal inertia of the radiator walls. Liso *et al.* [35] use a linear parametrization of the heat exchanger overall heat transfer coefficient as a function of the air flow rate. The coolant tank can also be modelled as done by Fly and Thring [114].

3.5. Condenser

Condensers can be present in some fuel cell systems where water recovery is important for water management, for instance in direct water injection humidification systems [115]. Condenser models with different degrees of complexity can be found in some works. Karnik *et al.* [26] model the condenser by a fixed liquid water removal efficiency. Striednig *et al.* consider [72] that the air at the exit of the condenser reaches a desired temperature, with 100 % relative humidity and no liquid water. Fly and Thring [38, 114] adopts an iterative model of the condenser which is able to predict both the heat transfer and the condensate rate. Their model is validated against experimental measurements. A 0D condenser model is also used by Schultze and Horn [29].

3.6. Inter-cooler

The inter-cooler is a heat exchanger placed after the compressor to reduce the air temperature before the air enters the membrane humidifier. Modelling the inter-cooler heat exchanger allows one to better describe the behavior of the temperature at the inlet of the membrane humidifier, and therefore the performance of this component. However, only few authors consider the inter-cooler in their models. Kim *et al.* [27] assumes that the temperature exiting the inter-cooler downstream the air compressor is constant and known. In Yang *et al.* [58] the temperature at the inlet of the dry side of the membrane humidifier is also considered to be constant and equal to 30 °C. Xing *et al.* [68] model the inter-cooler using a NTU-based method and a constant heat transfer coefficient. They show that the inter-cooler corresponds to less than 1 % in the thermal load of the cooling circuit.

3.7. Piping and manifolds

Finally, the different system components are connected by pipes and inlet/exhaust manifolds. Usually the pipes and manifolds between two components are lumped into a volume that behaves like a perfectly stirred tank, as proposed by Pukrushpan *et al.* [17]. Schultze and Horn [48] are the only authors that consider the time delay due to the flow speed in the pipe between different system components.

4. Model validation

Validation of fuel cell models is fundamental, specially as several more or less strong hypotheses are made to reduce the model complexity and computational cost. Most often, measurements of stack voltage and temperature are used to validate the models as obtaining them is straightforward. But for water management, quantities such as the water membrane content, water transport across the membrane, liquid water saturation, high-frequency resistance, outlet relative humidities and their spatial distribution and dynamics are of great importance. If accessing those quantities *in situ* remain difficult, some authors were able to validate their models with interesting data. Robin *et al.* [41] compared their model results to 2D current density and temperature distributions across the cell surface for three humidity conditions. The authors state that a good qualitative agreement is obtained, but note significant differences due to effects that are not accounted for in the model, such as a better electronic contact near the edges of the cell due to mechanical compression and bipolar plate welding. These effects are indeed shown to be significant by Liang *et al.* [116]. Tang *et al.* [49] and Gong *et al.* [70] also compared their model to current density distributions along the gas channel, obtaining very good agreement. Futter *et al.* [50] compared their model to electrochemical impedance spectra obtained at two different humidity conditions, but at a rather low current density of 0.2 A cm⁻². They suggest that the main deviations between their model and the experiments concern a capacitive peak around 1 Hz and are due to the gas concentration gradients along the channel direction, which are related to gas channel bends and not well represented by their model. Other authors compare their models

to measurements of the ohmic resistance [53, 58, 61, 70] or the ohmic losses [11], which is an indicator of the membrane resistance and therefore of its degree of hydration. Also, Liso *et al.* [46] and Falcão *et al.* [23] use respectively the cathode outlet mass flow rate and the net water transfer coefficient across the membrane for validation, while Salva *et al.* [47] validate their model against measurements of the fuel cell water content. To our knowledge, Headley *et al.* [45] are the only who validate their model against transient measurements of the relative humidity at the cathode outlet.

More commonly, authors use transient stack/cell voltage and temperature data to validate their model. [20, 25, 29, 36, 49, 53, 54, 58, 59, 61, 63, 69, 70]. A good example is the work of del Real *et al.* [20] where the validation is based on transient voltage and temperature data for three representative situations (fuel cell startup, flooding and variable load) with a Ballard Nexa 1.2 kW fuel cell system. Figure 5 shows the comparison for a variable load situation. Studies focused on cold start also use transient data for successful and failed fuel cell startup [25, 28, 49, 58, 70], such as the one in figure 6, extracted from Tang *et al.* [49]. Nevertheless, too many authors [19, 30, 33, 35, 38, 40, 42, 43, 66, 68] compare their models to static voltage measurements or polarization curves only, even if they are supposed to simulate transient effects. Worse, some authors, even in recent studies, do not present any validation of their models at all [26, 31, 56, 60]. This jeopardizes the reliability of fuel cell models, since several studies highlight the need for a validation methodology as comprehensive as possible [11, 117, 118].

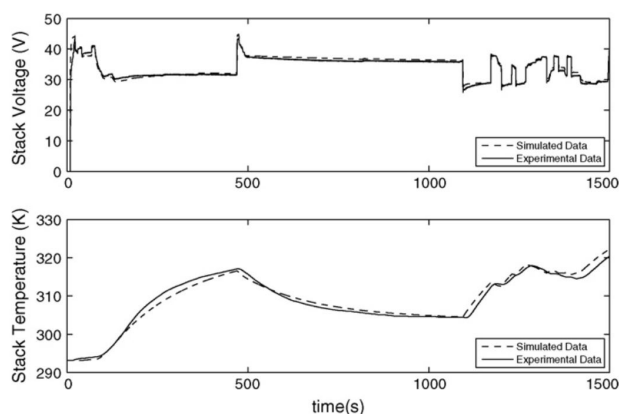


Fig. 5. Stack voltage and temperature results for a Ballard Nexa 1.2 kW fuel cell system under variable load: comparison between simulation and experimental data from Del Real *et al.* [20]. (Reproduced from Del Real *et al.* [20] with permission from Elsevier).

Some authors, compare different versions of their model to evaluate a given feature. Liso *et al.* [46] use this approach to show that considering non-equilibrium conditions for membrane water adsorption/desorption is needed to reproduce the experimental data. Futter *et al.* [50] compared a through-plane 1D version of their model with the original 1D+1D to show the impact of the along-the-channel gradients and to propose an explanation to the differences observed between their model and the EIS experimental data. The importance of the along-the-

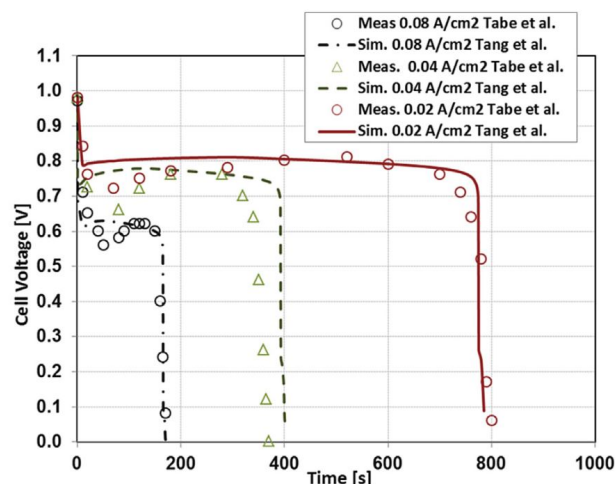


Fig. 6. Voltage break-in for the failed cold start of a fuel cell system: comparison between simulations from Tang *et al.* [49] and experimental data from Tabe *et al.* [119]. (Reproduced from Tang *et al.* [49] with permission from Elsevier).

channel discretization is also shown in the work of Headley *et al.* [45] by comparing their 1D model to its 0D version with a single control volume. Strahl *et al.* [36] compare their model to a simpler version which does not take into account the impact of the saturation on the catalyst active area, showing that the simpler model cannot reproduce the behavior observed experimentally. Beyond the validation of a model against experimental data, such a comparison between two (or more) versions of a model is a very good practice as it allows one to justify (or not) the need for a more complex model.

Concerning the validation of the models for other system auxiliaries, it is only present in some works as the focus is frequently on the fuel cell model. Kang *et al.* [40] validate their membrane humidifier and radiator models against steady-state experimental data. They use the dry side outlet dew point as a function of the air flow rate and temperature for the membrane humidifier and the heat rejection rate as a function of air and coolant mass flow rates for the radiator. Yang *et al.* [58] confront their models for different system components with experimental data. For the membrane humidifier model, they use data for the water vapor transfer rates as a function of the air flow rate and temperature and for the water recovery ratio as a function of the pressure and temperature. For the radiator, they use data for the coolant outlet temperature for different coolant and air mass flow rates. For the electrochemical hydrogen pump, they use the polarization curves for different CO_2/H_2 ratios. Such an extensive validation could be used as a benchmark for future system models. However, in general, validation of models for fuel cell system components deserve more attention, particularly for the transient behavior of components as the membrane humidifier or the radiator, which are fundamental for water and thermal management in most systems.

Another important aspect concerning validation is the use of benchmarks or standard conditions. Recently, Vetter and Schumacher [57] used operating conditions established by the Joint

Research Centre of the European Commission for automotive applications in an attempt to establish a baseline for model benchmark and validation. But the fuel cell modelling community still lacks a benchmark for model validation, as highlighted by the recent review of Zhao *et al.* [16], despite a long effort for the development of fuel cell models. The fact that few models are available as open-source also hinders their validation by the community, as explained by Weber *et al.* [14], as well as cross-validations between different models and the definition of a benchmark or reference model. Once again, Vetter and Schumacher [57] try to tackle the issue by proposing their model as an open-source, portable MATLAB file.

5. Computational time

Unfortunately, only few studies mention the computational time needed to run the proposed models. Yang *et al.* [58] only mention that its model is implemented in Matlab 2018a and run with a "powerful workstation". But after simplifications done by Gong *et al.* [70] their model, implemented in C, could be run 2 to 3 times faster than real-time on a computer with a 2.4 GHz processor. Goshtasbi *et al.* [61] implemented their model in C but used it as an S-Function in Simulink. They mention that their model runs about 50 times faster than real-time also on a computer with a 2.4 GHz processor for co-flow configurations and 2 or 3 times slower than that for counter-flow configurations, due to the iterative solution. The steady-state model of Salva *et al.* [47] takes less than 2 seconds to solve for around 20 steady-state operating points, which would make it 10 times faster than real time in a quasi-steady approach with a sampling period of 1 second. Schröder *et al.* [67] instead claim that their steady-state model can simulate several hundred points per second, while the model proposed by Vetter and Schumacher [57] would simulate only five points per second with the same computer. Xu *et al.* [69] mention that their model required 18 seconds to simulate 500 seconds of operation, making it around 30 times faster than real-time, whereas an equivalent 1D model would be 60 times slower. Ritzberger *et al.* [63] claim their model runs around 10 times faster than real time in a single-core personal laptop with a 2.6 GHz processor. The model of Headley *et al.* [45] took around 100 s to simulate 160 min with the along the channel discretization with six control volumes and ten times less in its 0D version with a single one. The fastest computational time reported is the one of Kang *et al.* [18], who states that their model runs 3000 times faster than real-time. The performances of those models are summarized in table 2.

6. Summary and perspectives

Throughout this review, we attempted to identify the modelling approaches and hypotheses commonly adopted in physics-based proton-exchange membrane fuel cell models that could be useful for system-level water and thermal management studies. We put in evidence the high diversity of approaches adopted in the literature concerning the cell voltage and the different overpotentials, the transport of gases, liquid water and

heat inside the cell, the spatial heterogeneity at the cell or the stack level and the dynamics of different phenomena. This diversity leads to models with different levels of computational efficiency (ranging from 1x to more than 50x faster than real-time), complexity and accuracy. But comparing the different models and modelling approaches in an objective way remain a very challenging task. Unfortunately, numerical implementations of most models are not openly available. Further, only very few works indicate clearly the computational time required to perform simulations with their models. Worse no standard validation benchmark exist. As system-level studies require models that are computationally efficient and validated against relevant experimental data, we believe that the development of standard validation procedure is an urgent matter. While most models described in this work concern only the fuel cell stack, some authors also present models for the system components, such as the compressor, the membrane humidifier or the cooling circuit radiator. Once again, in only few cases those models are validated.

Given the diversity of models already available in the literature, rather than developing new models from scratch, it would be more appropriate to select an existing model, perhaps adding some incremental changes. These incremental changes could then be verified by comparing the results with the ones of the original model. The selection of the existing model depends on the modelling goals and data availability. For instance, if predictive capabilities are required and detailed information about the cell materials are available, the model of Yang *et al.* [58] could be selected. The slip ratio parametrization proposed by Tang *et al.* [49] could be added to that model if liquid water transport in the gas channels is expected to be important. The consideration of platinum oxide growth dynamics proposed by Goshtasbi *et al.* [61] could be added if low-current regions are of interest. The model of Gong *et al.* [70] is an alternative if computational cost is an issue. If low information about the cell materials is available and the goal is to fit a computationally efficient model to operational data, the models developed by Schröder *et al.* [67] or Ritzberger *et al.* [64] may be the best. The model of Goshtasbi *et al.* [61] has a quite complex description of the catalyst layer and a high number of fitted parameters, while the interest of such complexity remains to be demonstrated. The network topology of the model proposed by Tang *et al.* [49] does not seem simple to implement at first sight. For steady-state investigations where detailed cell material data is available, Vetter and Schumacher [57] open model is an immediate choice. The model of Xu *et al.* [69] which uses analytical solutions of water and gas transport in the GDL can be a very interesting compromise between the capture of two-phase water dynamic effects and computational cost. However, its use require further validation on more diverse operating conditions. The model of Jiang *et al.* [11] can be used instead if dynamic effects are not of importance. Finally, the model of Xing *et al.* [68] is of interest when few data is available and the user is interested in thermal management at normal operating conditions (fully humidified membrane). To sum up, if several models with different levels of computational efficiency, complexity and accuracy are available in the literature, significant efforts

Table 2

Computational speed for different models as compared to real-time (RT).

1–5x faster than RT	5–50x faster than RT	> 50x faster than RT
Goshstasbi <i>et al.</i> [44]	Salva <i>et al.</i> [47]	Khan <i>et al.</i> [18]
Vetter and Schumacher [57]	Ritzberger <i>et al.</i> [63]	Headley <i>et al.</i> [45]
Gong <i>et al.</i> [70]	Goshstasbi <i>et al.</i> [61]	Schröder <i>et al.</i> [67]
	Xu <i>et al.</i> [69]	

are still needed to understand the impact of different modelling approaches and hypotheses. This can only be reached by extensive validation of the developed models against experimental data and against each other. That will lead to more reliable and efficient proton-exchange membrane fuel cell models, and as a consequence, more reliable and efficient system-level studies.

Acknowledgements

The author would like to thank Christian Beauger and Flavien Marteau for the proofreading of the manuscript and their valuable comments.

References

- [1] Y. Wang, D. F. Ruiz Diaz, K. S. Chen, Z. Wang, X. C. Adroher, Materials, technological status, and fundamentals of PEM fuel cells – a review, *Mater. Today* 32 (2020) 178–203. doi:10.1016/j.mattod.2019.06.005.
- [2] K. Jiao, X. Li, Water transport in polymer electrolyte membrane fuel cells, *Prog. Energy Combust. Sci.* 37 (3) (2011) 221–291. doi:10.1016/j.pecs.2010.06.002.
- [3] H. Li, Y. Tang, Z. Wang, Z. Shi, S. Wu, D. Song, J. Zhang, K. Fatih, J. Zhang, H. Wang, Z. Liu, R. Abouatallah, A. Mazza, A review of water flooding issues in the proton exchange membrane fuel cell, *J. Power Sources* 178 (1) (2008) 103–117. doi:10.1016/j.jpowsour.2007.12.068.
- [4] Q. Chen, G. Zhang, X. Zhang, C. Sun, K. Jiao, Y. Wang, Thermal management of polymer electrolyte membrane fuel cells: A review of cooling methods, material properties, and durability, *Appl. Energy* 286 (116496) (2021) 116496. doi:10.1016/j.apenergy.2021.116496.
- [5] Y. Luo, K. Jiao, Cold start of proton exchange membrane fuel cell, *Prog. Energy Combust. Sci.* 64 (2018) 29–61. doi:10.1016/j.pecs.2017.10.003.
- [6] S. T. Thompson, B. D. James, J. M. Huya-Kouadio, C. Houchins, D. A. DeSantis, R. Ahluwalia, A. R. Wilson, G. Kleen, D. Papageorgopoulos, Direct hydrogen fuel cell electric vehicle cost analysis: System and high-volume manufacturing description, validation, and outlook, *J. Power Sources* 399 (2018) 304–313. doi:10.1016/j.jpowsour.2018.07.100.
- [7] T. Jahnke, G. Futter, A. Latz, T. Malkow, G. Papakonstantinou, G. Tsotridis, P. Schott, M. Gérard, M. Quinaud, M. Quiroga, Others, Performance and degradation of proton exchange membrane fuel cells: State of the art in modeling from atomistic to system scale, *J. Power Sources* 304 (2016) 207–233.
- [8] M. Andersson, S. B. Beale, M. Espinoza, Z. Wu, W. Lehnert, A review of cell-scale multiphase flow modeling, including water management, in polymer electrolyte fuel cells, *Appl. Energy* 180 (2016) 757–778. doi:10.1016/j.apenergy.2016.08.010.
- [9] A. Goshtasbi, P. Garcia-Salaberri, J. Chen, K. Talukdar, D. G. Sanchez, T. Ersal, Through-the-Membrane transient phenomena in PEM fuel cells: A modeling study, *J. Electrochem. Soc.* 166 (7) (2019) F3154. doi:10.1149/2.0181907jes.
- [10] F. Nandjou, J.-P. Poirot-Crouvezier, M. Chandresris, Y. Bultel, A pseudo-3d model to investigate heat and water transport in large area PEM fuel cells – part 1: Model development and validation, *Int. J. Hydrogen Energy* 41 (34) (2016) 15545–15561. doi:10.1016/j.ijhydene.2016.05.117.
- [11] Y. Jiang, Z. Yang, K. Jiao, Q. Du, Sensitivity analysis of uncertain parameters based on an improved proton exchange membrane fuel cell analytical model, *Energy Convers. Manage.* 164 (2018) 639–654. doi:10.1016/j.enconman.2018.03.002.
- [12] R. Vetter, J. O. Schumacher, Experimental parameter uncertainty in proton exchange membrane fuel cell modeling. part i: Scatter in material parameterization, *J. Power Sources* 438 (2019) 227018. doi:10.1016/j.jpowsour.2019.227018.
- [13] R. Vetter, J. O. Schumacher, Experimental parameter uncertainty in proton exchange membrane fuel cell modeling. part II: Sensitivity analysis and importance ranking, *J. Power Sources* 439 (2019) 126529. doi:10.1016/j.jpowsour.2019.04.057.
- [14] A. Z. Weber, R. L. Borup, R. M. Darling, P. K. Das, T. J. Dursch, W. Gu, D. Harvey, A. Kusoglu, S. Litster, M. M. Mench, R. Mukundan, J. P. Owejan, J. G. Pharoah, M. Secanell, I. V. Zenyuk, A critical review of modeling transport phenomena in Polymer-Electrolyte fuel cells, *J. Electrochem. Soc.* 161 (12) (2014) F1254. doi:10.1149/2.0751412jes.
- [15] Q. Chen, Z. Niu, H. Li, K. Jiao, Y. Wang, Recent progress of gas diffusion layer in proton exchange membrane fuel cell: Two-phase flow and material properties, *Int. J. Hydrogen Energy* 46 (12) (2021) 8640–8671. doi:10.1016/j.ijhydene.2020.12.076.
- [16] J. Zhao, X. Li, C. Shum, J. McPhee, A review of physics-based and data-driven models for real-time control of polymer electrolyte membrane fuel cells, *Energy and AI* 6 (2021) 100114. doi:10.1016/j.egyai.2021.100114.
- [17] J. T. Pukrushpan, H. Peng, A. G. Stefanopoulou, Control-oriented modeling and analysis for automotive fuel cell systems, *J. Dyn. Syst. Meas. Control* 126 (1) (2004) 14–25. doi:10.1115/1.1648308.
- [18] M. J. Khan, M. T. Iqbal, Modelling and analysis of electro-chemical, thermal, and reactant flow dynamics for a PEM fuel cell system, *Fuel Cells* 5 (4) (2005) 463–475. doi:10.1002/fuce.200400072.
- [19] C. Bao, M. Ouyang, B. Yi, Modeling and control of air stream and hydrogen flow with recirculation in a PEM fuel cell system—i. control-oriented modeling, *Int. J. Hydrogen Energy* 31 (13) (2006) 1879–1896. doi:10.1016/j.ijhydene.2006.02.031.
- [20] A. J. del Real, A. Arce, C. Bordons, Development and experimental validation of a PEM fuel cell dynamic model, *J. Power Sources* 173 (1) (2007) 310–324. doi:10.1016/j.jpowsour.2007.04.066.
- [21] H. Huisseune, A. Willockx, M. De Paepe, Semi-empirical along-the-channel model for a proton exchange membrane fuel cell, *Int. J. Hydrogen Energy* 33 (21) (2008) 6270–6280. doi:10.1016/j.ijhydene.2008.08.013.
- [22] G. Vasu, A. K. Tangirala, Control-orientated thermal model for proton-exchange membrane fuel cell systems, *J. Power Sources* 183 (1) (2008) 98–108. doi:10.1016/j.jpowsour.2008.03.087.
- [23] D. S. Falcão, V. B. Oliveira, C. M. Rangel, C. Pinho, A. M. F. R. Pinto, Water transport through a PEM fuel cell: A one-dimensional model with heat transfer effects, *Chem. Eng. Sci.* 64 (9) (2009) 2216–2225. doi:10.1016/j.ces.2009.01.049.
- [24] D. Gerteisen, T. Heilmann, C. Ziegler, Modeling the phenomena of dehydration and flooding of a polymer electrolyte membrane fuel cell, *J. Power Sources* 187 (1) (2009) 165–181. doi:10.1016/j.jpowsour.2008.10.102.
- [25] K. Jiao, X. Li, Three-dimensional multiphase modeling of cold start pro-

- cesses in polymer electrolyte membrane fuel cells, *Electrochim. Acta* 54 (27) (2009) 6876–6891. doi:10.1016/j.electacta.2009.06.072.
- [26] A. Y. Karnik, J. Sun, A. G. Stefanopoulou, J. H. Buckland, Humidity and pressure regulation in a PEM fuel cell using a Gain-Scheduled static feedback controller, *IEEE Trans. Control Syst. Technol.* 17 (2) (2009) 283–297. doi:10.1109/TCST.2008.924562.
- [27] Y.-B. Kim, Improving dynamic performance of proton-exchange membrane fuel cell system using time delay control, *J. Power Sources* 195 (19) (2010) 6329–6341. doi:10.1016/j.jpowsour.2010.04.042.
- [28] M. Mangold, S. Piewek, O. Klein, A. Kienle, A model for the freeze start behavior of a PEM fuel cell stack, *J. Fuel Cell Sci. Technol.* 8 (3) (2011) 031006. doi:10.1115/1.4003015.
- [29] M. Schultze, J. Horn, A control oriented simulation model of an evaporation cooled polymer electrolyte membrane fuel cell system, *IFAC Proceedings Volumes* 44 (1) (2011) 14790–14795. doi:10.3182/20110828-6-IT-1002.00311.
- [30] C. Ziogou, S. Voutetakis, S. Papadopoulou, M. C. Georgiadis, Modeling, simulation and experimental validation of a PEM fuel cell system, *Comput. Chem. Eng.* 35 (9) (2011) 1886–1900. doi:10.1016/j.compchemeng.2011.03.013.
- [31] C. Damour, D. Grondin, M. Benne, B. Grondin-Perez, J. Deseure, J. P. Chabriat, Innovative model-based control approach of a proton exchange membrane fuel cell system, *J. Power Sources* 206 (2012) 144–152. doi:10.1016/j.jpowsour.2012.01.096.
- [32] E. Hosseinzadeh, M. Rokni, A. Rabbani, H. H. Mortensen, Thermal and water management of low temperature proton exchange membrane fuel cell in fork-lift truck power system, *Appl. Energy* 104 (2013) 434–444. doi:10.1016/j.apenergy.2012.11.048.
- [33] S. Chaudhary, V. K. Sachan, P. K. Bhattacharya, Two dimensional modelling of water uptake in proton exchange membrane fuel cell, *Int. J. Hydrogen Energy* 39 (31) (2014) 17802–17818. doi:10.1016/j.ijhydene.2014.08.128.
- [34] D. K. Kim, J. H. Seo, S. Kim, M. K. Lee, K. Y. Nam, H. H. Song, M. S. Kim, Efficiency improvement of a PEMFC system by applying a turbocharger, *Int. J. Hydrogen Energy* 39 (35) (2014) 20139–20150. doi:10.1016/j.ijhydene.2014.09.152.
- [35] V. Liso, M. P. Nielsen, S. K. Kær, H. H. Mortensen, Thermal modeling and temperature control of a PEM fuel cell system for fork-lift applications, *Int. J. Hydrogen Energy* 39 (16) (2014) 8410–8420. doi:10.1016/j.ijhydene.2014.03.175.
- [36] S. Strahl, A. Husar, P. Puleston, J. Riera, Performance improvement by temperature control of an Open-Cathode PEM fuel cell system, *Fuel Cells* 14 (3) (2014) 466–478. doi:10.1002/fuce.201300211.
- [37] Y. Zhou, Y. Luo, S. Yu, K. Jiao, Modeling of cold start processes and performance optimization for proton exchange membrane fuel cell stacks, *J. Power Sources* 247 (2014) 738–748. doi:10.1016/j.jpowsour.2013.09.023.
- [38] A. Fly, Thermal and water management of evaporatively cooled fuel cell vehicles, Ph.D. thesis, Loughborough University (2015).
- [39] S. Kang, Quasi-three dimensional dynamic modeling of a proton exchange membrane fuel cell with consideration of two-phase water transport through a gas diffusion layer, *Energy* 90 (2015) 1388–1400. doi:10.1016/j.energy.2015.06.076.
- [40] S. Kang, K. Min, Dynamic simulation of a fuel cell hybrid vehicle during the federal test procedure-75 driving cycle, *Appl. Energy* 161 (2016) 181–196. doi:10.1016/j.apenergy.2015.09.093.
- [41] C. Robin, M. Gerard, J. d’Arbigny, P. Schott, L. Jabbour, Y. Bultel, Development and experimental validation of a PEM fuel cell 2d-model to study heterogeneities effects along large-area cell surface, *Int. J. Hydrogen Energy* 40 (32) (2015) 10211–10230. doi:10.1016/j.ijhydene.2015.05.178.
- [42] X. Zhao, Y. Li, Z. Liu, Q. Li, W. Chen, Thermal management system modeling of a water-cooled proton exchange membrane fuel cell, *Int. J. Hydrogen Energy* 40 (7) (2015) 3048–3056. doi:10.1016/j.ijhydene.2014.12.026.
- [43] Z. Abidin, C. J. Webb, E. M. Gray, PEM fuel cell model and simulation in Matlab-Simulink based on physical parameters, *Energy* 116 (2016) 1131–1144. doi:10.1016/j.energy.2016.10.033.
- [44] A. Goshtasbi, B. L. Pence, T. Eرسال, Computationally efficient Pseudo-2D Non-Isothermal modeling of polymer electrolyte membrane fuel cells with Two-Phase phenomena, *J. Electrochem. Soc.* 163 (13) (2016) F1412. doi:10.1149/2.0871613jes.
- [45] A. Headley, V. Yu, R. Bordin, D. Chen, W. Li, Development and experimental validation of a Physics-Based PEM fuel cell model for cathode humidity control design (2016). doi:10.1109/tmech.2015.2505712.
- [46] V. Liso, S. Simon Araya, A. C. Olesen, M. P. Nielsen, S. K. Kær, Modeling and experimental validation of water mass balance in a PEM fuel cell stack, *Int. J. Hydrogen Energy* 41 (4) (2016) 3079–3092. doi:10.1016/j.ijhydene.2015.10.095.
- [47] J. A. Salva, A. Iranzo, F. Rosa, E. Tapia, Validation of cell voltage and water content in a PEM (polymer electrolyte membrane) fuel cell model using neutron imaging for different operating conditions, *Energy* 101 (2016) 100–112. doi:10.1016/j.energy.2016.02.006.
- [48] M. Schultze, J. Horn, Modeling, state estimation and nonlinear model predictive control of cathode exhaust gas mass flow for PEM fuel cells, *Control Eng. Pract.* 49 (2016) 76–86. doi:10.1016/j.conengprac.2016.01.006.
- [49] T. Tang, S. Heinke, A. Thüring, W. Tegethoff, J. Köhler, A spatially resolved fuel cell stack model with gas-liquid slip phenomena for cold start simulations, *Int. J. Hydrogen Energy* 42 (22) (2017) 15328–15346. doi:10.1016/j.ijhydene.2017.03.236.
- [50] G. A. Futter, P. Gazdzicki, K. A. Friedrich, A. Latz, T. Jahnke, Physical modeling of polymer-electrolyte membrane fuel cells: Understanding water management and impedance spectra, *J. Power Sources* 391 (2018) 148–161. doi:10.1016/j.jpowsour.2018.04.070.
- [51] Y. Qin, G. Liu, Y. Chang, Q. Du, Modeling and design of PEM fuel cell stack based on a flow network method, *Appl. Therm. Eng.* 144 (2018) 411–423. doi:10.1016/j.applthermaleng.2018.08.050.
- [52] L. Sun, J. Shen, Q. Hua, K. Y. Lee, Data-driven oxygen excess ratio control for proton exchange membrane fuel cell, *Appl. Energy* 231 (2018) 866–875. doi:10.1016/j.apenergy.2018.09.036.
- [53] B. Wang, K. Wu, Z. Yang, K. Jiao, A quasi-2d transient model of proton exchange membrane fuel cell with anode recirculation, *Energy Convers. Manage.* 171 (2018) 1463–1475. doi:10.1016/j.enconman.2018.06.091.
- [54] M. De Campo, Analysis and modeling of PEM fuel cell systems, Ph.D. thesis, Università degli Studi di Genova (2019).
- [55] J. Han, J. Hwang, S. Yu, A simulation of automotive fuel cell system for oxygen starvation trends by compressor surge under load follow-up, *Appl. Therm. Eng.* 154 (2019) 251–262. doi:10.1016/j.applthermaleng.2019.03.073.
- [56] A. L. Lazar, S. C. Konradt, H. Rottengruber, Open-Source dynamic Matlab/Simulink 1D proton exchange membrane fuel cell model, *Energies* 12 (18) (2019) 3478. doi:10.3390/en12183478.
- [57] R. Vetter, J. O. Schumacher, Free open reference implementation of a two-phase PEM fuel cell model, *Comput. Phys. Commun.* 234 (2019) 223–234. doi:10.1016/j.cpc.2018.07.023.
- [58] Z. Yang, Q. Du, Z. Jia, C. Yang, J. Xuan, K. Jiao, A comprehensive proton exchange membrane fuel cell system model integrating various auxiliary subsystems, *Appl. Energy* 256 (2019) 113959. doi:10.1016/j.apenergy.2019.113959.
- [59] Z. Yang, Q. Du, Z. Jia, C. Yang, K. Jiao, Effects of operating conditions on water and heat management by a transient multi-dimensional PEMFC system model, *Energy* 183 (2019) 462–476. doi:10.1016/j.energy.2019.06.148.
- [60] J. Chen, L. Huang, C. Yan, Z. Liu, A dynamic scalable segmented model of PEM fuel cell systems with two-phase water flow, *Math. Comput. Simul.* 167 (2020) 48–64. doi:10.1016/j.matcom.2018.05.006.
- [61] A. Goshtasbi, B. L. Pence, J. Chen, M. A. DeBolt, C. Wang, J. R. Waldecker, S. Hirano, T. Eرسال, A mathematical model toward Real-Time monitoring of automotive PEM fuel cells, *J. Electrochem. Soc.* 167 (2) (2020) 024518. doi:10.1149/1945-7111/ab6dd1.
- [62] J. Hoeflinger, P. Hofmann, Air mass flow and pressure optimisation of a PEM fuel cell range extender system, *Int. J. Hydrogen Energy* 45 (53) (2020) 29246–29258. doi:10.1016/j.ijhydene.2020.07.176.
- [63] D. Ritzberger, C. Hametner, S. Jakubek, A Real-Time dynamic fuel cell system simulation for Model-Based diagnostics and control: Validation on real driving data, *Energies* 13 (12) (2020) 3148. doi:10.3390/en13123148.

- [64] D. Ritzberger, J. Höflinger, Z. P. Du, C. Hametner, S. Jakubek, Data-driven parameterization of polymer electrolyte membrane fuel cell models via simultaneous local linear structured state space identification, *Int. J. Hydrogen Energy* 46 (21) (2021) 11878–11893. doi:10.1016/j.ijhydene.2021.01.037.
- [65] Y. Wang, J. Li, Q. Tao, M. H. S. Bargal, M. Yu, X. Yuan, C. Su, Thermal management system modeling and simulation of a Full-Powered fuel cell vehicle, *J. Energy Res. Technol.* 142 (6) (2020) 061304. doi:10.1115/1.4045479.
- [66] H. Fu, J. Shen, L. Sun, K. Y. Lee, Fuel cell humidity modeling and control using cathode internal water content, *Int. J. Hydrogen Energy* 46 (15) (2021) 9905–9917. doi:10.1016/j.ijhydene.2020.04.283.
- [67] M. Schröder, F. Becker, J. Kallo, C. Gentner, Optimal operating conditions of PEM fuel cells in commercial aircraft, *Int. J. Hydrogen Energy* 46 (66) (2021) 33218–33240. doi:10.1016/j.ijhydene.2021.07.099.
- [68] L. Xing, H. Chang, R. Zhu, T. Wang, Q. Zou, W. Xiang, Z. Tu, Thermal analysis and management of proton exchange membrane fuel cell stacks for automotive vehicle, *Int. J. Hydrogen Energy* 46 (64) (2021) 32665–32675. doi:10.1016/j.ijhydene.2021.07.143.
- [69] L. Xu, Z. Hu, C. Fang, L. Xu, J. Li, M. Ouyang, A reduced-dimension dynamic model of a proton-exchange membrane fuel cell, *Int. J. Energy Res.* 45 (12) (2021) 18002–18017. doi:10.1002/er.6945.
- [70] Z. Gong, B. Wang, K. Wu, T. Miao, K. Yang, S. Zhai, R. Ma, F. Gao, K. Jiao, A 1 + 1-D multiphase proton exchange membrane fuel cell model for Real-Time simulation, *IEEE Transactions on Transportation Electrification* 8 (2) (2022) 2928–2944. doi:10.1109/TTE.2021.3115794.
- [71] M. Striednig, M. Cochet, P. Boillat, T. J. Schmidt, F. N. Büchi, A model based investigation of evaporative cooling for polymer electrolyte fuel cells – stack level analysis, *J. Power Sources* 517 (2022) 230706. doi:10.1016/j.jpowsour.2021.230706.
- [72] M. Striednig, T. J. Schmidt, F. N. Büchi, A model based investigation of evaporative cooling for polymer electrolyte fuel cells – system level analysis, *J. Power Sources* 542 (2022) 231720. doi:10.1016/j.jpowsour.2022.231720.
- [73] J. C. Amphlett, R. M. Baumert, R. F. Mann, B. A. Peppley, P. R. Roberge, T. J. Harris, Performance modeling of the Ballard mark IV solid polymer electrolyte fuel cell: I. mechanistic model development, *J. Electrochem. Soc.* 142 (1) (1995) 1. doi:10.1149/1.2043866.
- [74] T. E. Springer, T. A. Zawodzinski, S. Gottesfeld, Polymer electrolyte fuel cell model, *J. Electrochem. Soc.* 138 (8) (1991) 2334. doi:10.1149/1.2085971.
- [75] R. F. Mann, J. C. Amphlett, M. A. I. Hooper, H. M. Jensen, B. A. Peppley, P. R. Roberge, Development and application of a generalised steady-state electrochemical model for a PEM fuel cell, *J. Power Sources* 86 (1) (2000) 173–180. doi:10.1016/S0378-7753(99)00484-X.
- [76] A. Z. Weber, J. Newman, A theoretical study of membrane constraint in polymer-electrolyte fuel cells, *AIChE J.* 50 (12) (2004) 3215–3226. doi:10.1002/aic.10230.
- [77] P. Zihrl, I. Hartung, S. Kirsch, G. Huebner, F. Hasché, H. A. Gasteiger, Voltage cycling induced losses in electrochemically active surface area and in H₂/air-performance of PEM fuel cells, *J. Electrochem. Soc.* 163 (6) (2016) F492–F498. doi:10.1149/2.0561606jes.
- [78] M. Zago, A. Baricci, A. Bisello, T. Jahnke, H. Yu, R. Maric, P. Zelenay, A. Casalegno, Experimental analysis of recoverable performance loss induced by platinum oxide formation at the polymer electrolyte membrane fuel cell cathode, *J. Power Sources* 455 (2020) 227990. doi:10.1016/j.jpowsour.2020.227990.
- [79] D. Bernhard, T. Kadyk, U. Krewer, S. Kirsch, How platinum oxide affects the degradation analysis of PEM fuel cell cathodes, *Int. J. Hydrogen Energy* 46 (26) (2021) 13791–13805. doi:10.1016/j.ijhydene.2021.01.058.
- [80] L. Hao, K. Moriyama, W. Gu, C.-Y. Wang, Modeling and experimental validation of Pt loading and electrode composition effects in PEM fuel cells, *J. Electrochem. Soc.* 162 (8) (2015) F854. doi:10.1149/2.0221508jes.
- [81] M. Lindstrom, B. Wetton, A comparison of Fick and Maxwell–Stefan diffusion formulations in PEMFC gas diffusion layers, *Heat Mass Transfer.* 53 (1) (2017) 205–212. doi:10.1007/s00231-016-1812-7.
- [82] J. Park, X. Li, An experimental and numerical investigation on the cross flow through gas diffusion layer in a PEM fuel cell with a serpentine flow channel, *J. Power Sources* 163 (2) (2007) 853–863. doi:10.1016/j.jpowsour.2006.09.083.
- [83] Y. Wang, K. S. Chen, Elucidating two-phase transport in a polymer electrolyte fuel cell, part 1: Characterizing flow regimes with a dimensionless group, *Chem. Eng. Sci.* 66 (15) (2011) 3557–3567. doi:10.1016/j.ces.2011.04.016.
- [84] K. S. Udell, Heat transfer in porous media considering phase change and capillarity—the heat pipe effect, *Int. J. Heat Mass Transf.* 28 (2) (1985) 485–495. doi:10.1016/0017-9310(85)90082-1.
- [85] M. C. Leverett, Capillary behavior in porous solids, *Trans. Soc. Pet. Eng. Am. Inst. Min. Metall. Pet. Eng. Inc* 142 (01) (1941) 152–169. doi:10.2118/941152-g.
- [86] J. T. Gostick, M. A. Ioannidis, M. W. Fowler, M. D. Pritzker, Wettability and capillary behavior of fibrous gas diffusion media for polymer electrolyte membrane fuel cells, *J. Power Sources* 194 (1) (2009) 433–444. doi:10.1016/j.jpowsour.2009.04.052.
- [87] E. C. Kumbur, K. V. Sharp, M. M. Mench, Validated leverett approach for multiphase flow in PEFC diffusion media: II. compression effect, *J. Electrochem. Soc.* 154 (12) (2007) B1305. doi:10.1149/1.2784285.
- [88] T. Tang, S. Heinke, A. Thüring, W. Tegethoff, J. Köhler, Freeze start drive cycle simulation of a fuel cell powertrain with a two-phase stack model and exergy analysis for thermal management improvement, *Appl. Therm. Eng.* 130 (2018) 637–659. doi:10.1016/j.applthermaleng.2017.10.100.
- [89] J. Hu, J. Li, L. Xu, F. Huang, M. Ouyang, Analytical calculation and evaluation of water transport through a proton exchange membrane fuel cell based on a one-dimensional model, *Energy* 111 (2016) 869–883. doi:10.1016/j.energy.2016.06.020.
- [90] Y. Huang, X. Xiao, H. Kang, J. Lv, R. Zeng, J. Shen, Thermal management of polymer electrolyte membrane fuel cells: A critical review of heat transfer mechanisms, cooling approaches, and advanced cooling techniques analysis, *Energy Convers. Manage.* 254 (2022) 115221. doi:10.1016/j.enconman.2022.115221.
- [91] Y. Wang, H. Yuan, A. Martinez, P. Hong, H. Xu, others, Polymer electrolyte membrane fuel cell and hydrogen station networks for automobiles: Status, technology, and perspectives, *Advances in Applied* (2021).
- [92] M. Sauermoser, S. Kjelstrup, B. G. Pollet, The impact of peltier and dufour coefficients on heat fluxes and temperature profiles in the polymer electrolyte fuel cells, *J. Electrochem. Soc.* 167 (14) (2020) 144503. doi:10.1149/1945-7111/abc110.
- [93] S. Strahl, R. Costa-Castelló, Model-based analysis for the thermal management of open-cathode proton exchange membrane fuel cell systems concerning efficiency and stability, *J. Process Control* 47 (2016) 201–212. doi:10.1016/j.jprocont.2016.09.004.
- [94] E. Padgett, N. Andrejevic, Z. Liu, A. Kongkanand, W. Gu, K. Moriyama, Y. Jiang, S. Kumaraguru, T. E. Moylan, R. Kukreja, D. A. Muller, Editors’ Choice—Connecting fuel cell catalyst nanostructure and accessibility using quantitative Cryo-STEM tomography, *J. Electrochem. Soc.* 165 (3) (2018) F173. doi:10.1149/2.0541803jes.
- [95] A. Kusoglu, A. Z. Weber, New insights into perfluorinated Sulfonic-Acid ionomers, *Chem. Rev.* 117 (3) (2017) 987–1104. doi:10.1021/acs.chemrev.6b00159.
- [96] E. J. F. Dickinson, G. Smith, Modelling the Proton-Conductive membrane in practical polymer electrolyte membrane fuel cell (PEMFC) simulation: A review, *Membranes* 10 (11) (Oct. 2020). doi:10.3390/membranes10110310.
- [97] A. Z. Weber, J. Newman, Transport in Polymer-Electrolyte membranes: I. physical model, *J. Electrochem. Soc.* 150 (7) (2003) A1008. doi:10.1149/1.1580822.
- [98] P. W. Majsztrik, M. B. Satterfield, A. B. Bocarsly, J. B. Benziger, Water sorption, desorption and transport in nafion membranes, *J. Memb. Sci.* 301 (1) (2007) 93–106. doi:10.1016/j.memsci.2007.06.022.
- [99] M. Koz, S. G. Kandlikar, Numerical investigation of interfacial transport resistance due to water droplets in proton exchange membrane fuel cell air channels, *J. Power Sources* 243 (2013) 946–957. doi:10.1016/j.jpowsour.2013.06.075.
- [100] M. Koz, S. G. Kandlikar, Interfacial oxygen transport resistance in a proton exchange membrane fuel cell air channel with an array of water droplets, *Int. J. Heat Mass Transf.* 80 (2015) 180–191. doi:10.1016/

- [j.ijheatmasstransfer.2014.08.079](#).
- [101] M. Koz, S. G. Kandlikar, Oxygen transport resistance at gas diffusion layer – air channel interface with film flow of water in a proton exchange membrane fuel cell, *J. Power Sources* 302 (2016) 331–342. doi:10.1016/j.jpowsour.2015.10.080.
- [102] T. Miao, C. Tongsh, J. Wang, P. Cheng, J. Liang, Z. Wang, W. Chen, C. Zhang, F. Xi, Q. Du, B. Wang, F. Bai, K. Jiao, Current density and temperature distribution measurement and homogeneity analysis for a large-area proton exchange membrane fuel cell, *Energy* 239 (2022) 121922. doi:10.1016/j.energy.2021.121922.
- [103] M. Zaglio, J. Roth, A. Wokaun, J. Mantzaras, F. N. Büchi, Transient Bi-Domain 1D PEFC model, *ECS Electrochem. Lett.* 1 (1) (2012) F1. doi:10.1149/2.003201eel.
- [104] A. Z. Weber, Effective diffusion-medium thickness for simplified polymer-electrolyte-fuel-cell modeling, *Electrochim. Acta* 54 (2) (2008) 311–315. doi:10.1016/j.electacta.2008.07.084.
- [105] Y. Li, P. Pei, Z. Ma, P. Ren, H. Huang, Analysis of air compression, progress of compressor and control for optimal energy efficiency in proton exchange membrane fuel cell, *Renewable Sustainable Energy Rev.* 133 (2020) 110304. doi:10.1016/j.rser.2020.110304.
- [106] D. Chen, W. Li, H. Peng, An experimental study and model validation of a membrane humidifier for PEM fuel cell humidification control, *J. Power Sources* 180 (1) (2008) 461–467. doi:10.1016/j.jpowsour.2008.02.055.
- [107] S. Park, D. Jung, Effect of operating parameters on dynamic response of water-to-gas membrane humidifier for proton exchange membrane fuel cell vehicle, *Int. J. Hydrogen Energy* 38 (17) (2013) 7114–7125. doi:10.1016/j.ijhydene.2013.03.170.
- [108] M. P. Nielsen, A. C. Olesen, A. Menard, Modeling of a membrane based humidifier for fuel cell applications subject to end-of-life conditions, in: *Proceedings from The 55th Conference on Simulation and Modelling*, 2014, pp. 1–10.
- [109] D. Bhatia, M. Sabharwal, C. Duell, Analytical model of a membrane humidifier for polymer electrolyte membrane fuel cell systems, *Int. J. Heat Mass Transf.* 58 (1) (2013) 702–717. doi:10.1016/j.ijheatmasstransfer.2012.11.033.
- [110] D. Kadylak, P. Cave, W. Mérida, Effectiveness correlations for heat and mass transfer in membrane humidifiers, *Int. J. Heat Mass Transf.* 52 (5) (2009) 1504–1509. doi:10.1016/j.ijheatmasstransfer.2008.09.002.
- [111] D. Kadylak, W. Mérida, Experimental verification of a membrane humidifier model based on the effectiveness method, *J. Power Sources* 195 (10) (2010) 3166–3175. doi:10.1016/j.jpowsour.2009.12.005.
- [112] E. McCarthy, S. Flick, W. Mérida, Response surface methods for membrane humidifier performance, *J. Power Sources* 239 (2013) 399–408. doi:10.1016/j.jpowsour.2013.04.002.
- [113] J. Han, J. Feng, P. Chen, Y. Liu, X. Peng, A review of key components of hydrogen recirculation subsystem for fuel cell vehicles, *Energy Conversion and Management: X* 15 (2022) 100265. doi:10.1016/j.ecmx.2022.100265.
- [114] A. Fly, R. H. Thring, A comparison of evaporative and liquid cooling methods for fuel cell vehicles, *Int. J. Hydrogen Energy* 41 (32) (2016) 14217–14229. doi:10.1016/j.ijhydene.2016.06.089.
- [115] Y. Chang, Y. Qin, Y. Yin, J. Zhang, X. Li, Humidification strategy for polymer electrolyte membrane fuel cells – a review, *Appl. Energy* 230 (2018) 643–662. doi:10.1016/j.apenergy.2018.08.125.
- [116] P. Liang, D. Qiu, L. Peng, P. Yi, X. Lai, J. Ni, Contact resistance prediction of proton exchange membrane fuel cell considering fabrication characteristics of metallic bipolar plates, *Energy Convers. Manage.* 169 (2018) 334–344. doi:10.1016/j.enconman.2018.05.069.
- [117] C. H. Min, Y. L. He, X. L. Liu, B. H. Yin, W. Jiang, W. Q. Tao, Parameter sensitivity examination and discussion of PEM fuel cell simulation model validation: Part II: Results of sensitivity analysis and validation of the model, *J. Power Sources* 160 (1) (2006) 374–385. doi:10.1016/j.jpowsour.2006.01.080.
- [118] B. Xie, M. Ni, G. Zhang, X. Sheng, H. Tang, Y. Xu, G. Zhai, K. Jiao, Validation methodology for PEM fuel cell three-dimensional simulation, *Int. J. Heat Mass Transf.* 189 (2022) 122705. doi:10.1016/j.ijheatmasstransfer.2022.122705.
- [119] Y. Tabe, M. Saito, K. Fukui, T. Chikahisa, Cold start characteristics and freezing mechanism dependence on start-up temperature in a polymer electrolyte membrane fuel cell, *J. Power Sources* 208 (2012) 366–373. doi:10.1016/j.jpowsour.2012.02.052.